論文 / 著書情報
Article / Book Information

Title	Reliability assessment of the performance of granular column in the nonuniform liquefiable ground to mitigate the liquefaction-induced ground deformation
Authors	Ritesh Kumar, Akihiro Takahashi
Citation	Georisk: Assessment and Management of Risk for Engineered Systems and Geohazards, Vol. 16, No. 2, pp. 376-395
Pub. date	2022, 5
DOI	https://doi.org/10.1080/17499518.2020.1836378
Creative Commons	See next page.
Note	This is an Accepted Manuscript version of the following article, accepted for publication in Georisk: Assessment and Management of Risk for Engineered Systems and Geohazards. [Ritesh Kumar, Akihiro Takahashi, (2022), Reliability assessment of the performance of granular column in the nonuniform liquefiable ground to mitigate the liquefaction-induced ground deformation, Georisk: Assessment and Management of Risk for Engineered Systems and Geohazards, Vol. 16, No. 2, pp. 376-395, https://doi.org/10.1080/17499518.2020.1836378]. It is deposited under the terms of the Creative Commons Attribution-NonCommercial-NoDerivatives License (http://creativecommons.org/licenses/by-nc-nd/4.0/), which permits non-commercial re-use, distribution, and reproduction in any medium, provided the original work is properly cited, and is not altered, transformed, or built upon in any way.

License

Reliability assessment of the performance of granular column in the nonuniform liquefiable ground to mitigate the liquefaction-induced ground deformation

Ritesh Kumar and Akihiro Takahashi*

Department of Civil and Environmental Engineering,

Tokyo Institute of Technology, Japan

*Corresponding author

Email: takahashi.a.al@m.titech.ac.jp

Tel: +81-(0)3-5734-2593 Fax: +81-(0)3-5734-3577

Georisk: Assessment and Management of Risk for Engineered Systems and Geohazards, 16(2), 376-395, 2021

Official URL:

https://doi.org/10.1080/17499518.2020.1836378

Abstract

Granular columns have been widely used to mitigate the liquefaction-induced ground deformation. The increment in lateral stress due to densification, shear reinforcement, and drainage capacity of granular columns are believed to increase the liquefaction resistance of the ground. However, several case histories and recent research development exhibited the limitations of the effectiveness of granular columns under strong earthquakes. Besides, the mechanism of shear reinforcement governed by granular columns is poorly understood. Moreover, the spatial nonuniformity of the ground should be considered for a reliable engineering assessment of the performance of granular columns. A series of three-dimensional nonlinear stochastic analyses are carried out using the OpenSees framework with PDMY02 elasto-plastic soil constitutive model to map the reliability of the performance of equally-spaced granular columns. Soil variability is implemented with stochastic realizations of overburden and energy-corrected, equivalent clean sand, $(N1)_{60cs}$ values using spatially correlated Gaussian random field. The reliability of the performance of granular column is assessed based on the stochastic distributions of average surface settlement and horizontal ground displacement associated with the degree of confidence. The implications of cumulative absolute velocity, Arias Intensity and peak acceleration of different ground motions on the efficacy of the granular column are also discussed.

Keywords: Granular column; liquefaction; spatial nonuniformity; stochastic analyses

1. Introduction

Liquefaction has caused severe damage to the built environment, for instance, settlement, tilting, and sinking of the foundation-structure system all over the world during many past earthquakes. The construction on the liquefiable ground is not recommended unless the appropriate liquefaction mitigation measures are taken at such sites. Liquefaction mitigation by granular columns or gravel drainage system is one of the well-established techniques, which is used to facilitate quick dissipation of excess pore water pressure generated during the earthquake. Besides, the granular columns densify the surrounding soil during installation and believe to re-distribute the earthquake-induced or pre-existing stresses (Seed and booker 1977, Tokimatsu et al. 1990, and Adalier and Elgamal 2004).

Many researchers have found that the pioneering design charts for granular columns developed by Seed and Booker (1977) overestimate their performance (Boulanger et al. 1998, Adalier et al. 2003, Adalier and Elgamal 2004, Olarte et al. 2017, and Kumar et al. 2019b). Brennan and Madabhushi (2002) performed centrifuge experiments to investigate the effectiveness of vertical drains in the mitigation of liquefaction-induced effects. They reported that the flow front (zone of adequate drainage at any time) play a vital role in the performance of gravel drains. The flow front slows down with distance from the gravel drain, and hence it is highly relevant to consider the effective radius and adequate spacing between the gravel drains. Adalier and Elgamal (2004) have performed centrifuge experiments to understand the liquefaction mitigation capabilities of granular columns and associated ground deformations. They concluded that the performance of granular columns depends on their drainage capacity, and the densification of the ground during the installation of granular columns is inevitable. The ancillary benefits of treating the ground with granular columns are the restriction of shear deformation, offering the containment of the encapsulated soil, and providing stiffening-matrix effects (reducing

the stress in adjacent soil) (Boulanger et al. 1998, Adalier et al. 2003, Adalier and Elgamal 2004, Olarte et al. 2017, and Kumar et al. 2019b). However, these effects are not well established yet, and more research is needed for a better understanding in this regard. Raymajhi et al. (2016) investigated the contribution mechanism of shear reinforcement, increment in lateral stress, and drainage effects with the help of three-dimensional finite-element analyses. They reported that the granular columns undergo a shear strain deformation pattern, which is noncompatible with the surrounding soil contrasting with the conventional design assumption of shear strain compatibility. Many researchers (Goughnour and Pestana 1998, Green et al. 2008, Olgun and Martin 2008, and Raymajhi et al. 2014) also suggested that the granular columns may deform in both flexure and shear modes which are not considered in the conventional design charts.

The ground is prone to spatial nonuniformity and needs to be taken into account for a reliable engineering assessment of the performance of granular columns. The modeling of inherent soil variability can be achieved utilizing the advanced nonlinear finite element analyses and well-calibrated sophisticated elasto-plastic soil constitutive models. Reliability analyses provide a means of evaluating the combined effects of uncertainties in the parameters involved in the calculations, and they offer a useful supplement to traditional engineering judgment (Duncan 2000). For a thorough understanding of risk and reliability analyses in geotechnical engineering, readers are suggested to read Christian et al. (1994) and Phoon and Ching (2014). Case histories and recent research development have exhibited the limitations of granular columns under strong earthquakes (Boulanger et al. 1998, Adalier et al. 2003, Adalier and Elgamal 2004, Brennan and Madabhushi 2002, Olarte et al. 2017, and Kumar et al. 2019b). Moreover, the mechanism of liquefaction resistance, drainage effects, deformation pattern, and shear reinforcement due to granular columns are poorly understood. In this paper, a series of nonlinear stochastic analyses are carried out using the OpenSees framework with PDMY02 elasto-

plastic soil constitutive model. The soil variability is implemented with stochastic realizations of overburden and energy-corrected, equivalent clean sand, $(N1)_{60cs}$ values using spatially correlated Gaussian random field. Three-dimensional finite element simulations are performed for the sufficient number of realizations to map the reliability of the effectiveness of equally-spaced granular columns to mitigate the liquefaction-induced ground deformation.

2. Numerical model

The presented work is inspired by the findings of a series of centrifuge experiments reported in Kumar et al. (2019b). The authors developed a hybrid foundation, which is a combination of the gravel drainage system and friction piles as a remedial measure against the liquefaction-induced effects. The efficacy of the hybrid foundation was investigated in the uniform deposit of liquefiable Toyoura sand (D_R ~50%). The gravel drainage system (D_R ~30%) used in the centrifuge experiment was an array of 5x5 granular columns (see Figure 1). Design charts reported by Seed and Booker (1977) in their seminal work and the revised guidelines presented by Bouckovalas et al. (2006) were used to design the granular columns. Many parameters, e.g., replacement area, target excess pore water pressure ratio, earthquake intensity, reported case histories, and installation methodology of gravel drains, were considered while designing the granular columns. The index properties of Toyoura sand and granular column (silica no. 3) are shown in Table 1.

There are a few parameters that need to be considered to ensure the reliability of the performance of the granular column as an integral part of the developed hybrid foundation. For instance, the ground is prone to spatial nonuniformity, which was not considered in the centrifuge experiments. Besides, the granular columns only provided additional drainage to rapidly dissipate the excess pore water pressure, and the

77 contribution in the shear reinforcement was ignored in the centrifuge experiments.
78 Moreover, the density of granular columns in the centrifuge experiments was ~30%,
79 which is significantly less than the density of constructed granular columns at the site
80 (which is usually in the range of 75~85%). These site-specific parameters are essential to
81 consider for a reliable engineering judgment on the performance of granular columns to
82 mitigate the liquefaction-induced ground deformation. For that purpose, half of the single
83 granular column (with D_R ~80%) in the middle of the gravel drainage system (due to
84 symmetry) under the buffer tank (BT) and associated model ground (effective drainage
85 zone of granular column) in the above-mentioned centrifuge test is considered for the
86 numerical simulations, as shown in Figure 2. The reason for this idealization is that the
87 modeling of the whole centrifuge model and gravel drainage system (see Figure 1) is
88 computationally expensive and not feasible for stochastic analyses as the reliability
89 assessment requires thousands of analyses. Similar idealizations have been well-adopted
90 by many researchers (Elgamal et al. 2009, Raymajhi et al. 2014, and Khosravifar et al.
91 2018). This approach does not account for the distinct stress distribution to the individual
92 granular column (in the gravel drainage system) coming from the foundation-structure
93 system during the dynamic event. Instead, the intent is to explore the reliability at a single
94 granular column to get an insight into the overall performance of the whole gravel
95 drainage system.
96 Numerical simulations are carried with Rayleigh damping of 1% at a frequency of
97 1 Hz corresponding to the first-mode of a typical nonlinear ground response is used in the
98 analyses (Stewart et al., 2008). The ground is modeled using brick u-p (8-node brickUP)
99 elements. The load from the foundation-structure system is modeled as surface pressure
100 for simplicity. The effects of the superstructure inertia are ignored in this study. The
101 bottom nodes of the ground are kept fixed in all the degrees of freedom. Tokachi-Oki
102 ground motion (NS component of recorded shaking at the Hachinohe Port in 1968, see

Figure 2) is imposed on the bottom nodes of the ground during the dynamic analyses using the multiple support excitation technique in OpenSees. All the nodes on the side boundary with the same elevation are tied to move together (in X and Y direction) using equalDOF command in OpenSees. The vertical movement of side boundary nodes are kept free. The nonuniformity of the liquefiable ground is considered in the presented study. Based on the random realization of the nonuniformity of the ground, the relative density of the elements would fall into a wide range (D_R = 30 – 75%, discussed in subsection 4.1). The dynamic behavior of the liquefiable element significantly depends on the relative density and its corresponding calibrated parameters. In this case, tie the vertical movement of side nodes with periodic boundary (as adopted by Law and Lam, 2001; Elgamal et al., 2009; and Rayamajhi et al., 2014, for a uniform ground) would enforce the side boundary elements to have same settlement which is not reasonable for the nonuniform ground even though the extent of the model in the X and Y directions (see Figure 2) are small compared to the size of the granular column. All the nodes above the water table are assigned zero pore water pressure. The nodes of the planes of Y= 0 and 0.7 m (see Figure 2) are kept fixed against the out-of-plane displacement.

PDMY02 soil constitutive model is used to model the dynamic behavior of the ground. The PDMY02 Model is an elastoplastic soil-liquefaction constitutive model originally developed to simulate the cyclic liquefaction response and the associated accumulation of cyclic shear deformation in clean sand and silt (Yang et al. 2003). Within a stress–space plasticity framework, PDMY02 Model employs a new flow rule and strain–space parameters to simulate the cyclic development and evolution of plastic shear strain. PDMY02 does not include a critical state soil mechanics framework.

The parameters of the PDMY02 Model are calibrated to achieve the single-amplitude shear strain of 3% in cyclic undrained simple shear loading with zero initial static shear stress ratio on a horizontal plane at a single element level. Laboratory test

129 results from Chiaro et al. (2012) are considered as the dynamic behavior of saturated
130 Toyoura sand with a relative density of 50% at a single element level for the calibration
131 purpose. Figure 3(a) shows a typical response of calibrated PDMY02 Model for cyclic
132 stress ratio (CSR) = 0.171, D_R = 50%, and σ'_{vc} = 100 kPa in cyclic undrained simple shear
133 loading with zero initial static shear stress ratio on a horizontal plane. The PDMY02
134 Model exhibits the ability of shear strain accumulation, commonly referred to as cyclic
135 mobility, which is evident from the stress-strain behavior. The stress path is shown in
136 Figure 3(b). The vertical effective stress ratio drops down to nearly zero within 15 cycles
137 and triggered large shear strains afterward. Numerically simulated cyclic response at the
138 single element level is obtained after calibrating the parameters of the PDMY02 Model
139 to achieve a similar response as observed in the experiment in terms of cyclic mobility,
140 initial shear modulus, and the accumulation rate of shear strain. Figure 3(c) shows the
141 shear strain accumulation with the drop in vertical effective stress ratio. Figure 3(d) shows
142 the CSR curves corresponding to single-amplitude shear strains of 3% with zero initial
143 static shear stress ratio. The calibrated values of the PDMY02 Model for Toyoura sand
144 (D_R ~50%) and granular column (D_R ~80%) are shown in Table 2.

145 ## 3. Deterministic analyses

146 ### *3.1 Ground deformation*

147 The deterministic analysis is carried out (Toyoura sand with D_R = 50%, the granular
148 column with D_R = 80%) before performing the series of stochastic analyses to investigate
149 the dynamic behavior of a liquefiable ground treated with equally-spaced granular
150 columns. The simulated time histories of average settlement of the top surface of the
151 grounds with and without granular column are shown in Figure 4. The settlement time
152 histories are divided into co-shaking and post-shaking phases. It is evident that the rate of
153 settlement in the co-shaking phase (until t = 50 s) is significantly large in the case of the

ground with the granular column in comparison with the ground without a granular column. The large permeability of the granular column seems to adversely affect the settlement evolution during the co-shaking phase. The settlement time histories also indicate that the relatively large stiffness of the granular column (with respect to the ground) does not have any contribution in the restriction of the average vertical settlement of the top surface of the ground. The authors also confirmed this with the simulated settlement time histories of the ground with granular columns of density D_R = 30 and 80% and found that there was not any considerable change in the simulated settlement response. The effectiveness of the granular column is evident in restricting the post-shaking average settlement of the top surface of the ground. Similar trends were observed in the centrifuge experiments (Kumar et al. 2019b). However, the numerically simulated settlement is significantly less than the observed settlement (in centrifuge experiments) in the post-shaking phase for both the grounds with and without granular column, while that in the co-shaking is comparable to the observed ones. It is to be noted that the laminar boundary conditions in the numerical model ignore the settlement contribution due to three-dimensional lateral spreading in the centrifuge test. This idealization is also responsible for the overall less settlement in the case of numerical simulations. Several researchers (Taibet et al. 2007; Dashti and Bray 2013; Karimi and Dashti 2015; and Kumar et al. 2020) have made similar observations. The numerical models typically exhibit limitations in capturing the settlement caused by partial drainage and reconsolidation specifically in the post-shaking phase because of the characteristics of their constitutive formulations, as reported by Shahir et al. (2012), Karimi and Dashti (2016), Boulanger and Ziotopoulou (2017), and Adamidis and Madabhushi (2019).

Figure 5 shows the horizontal displacement of the top surface of the grounds with and without the granular column. The peaks of applied ground motion triggered the large horizontal displacement at the beginning of the shaking (t = 12 ~ 16 s). The ground

without the granular column experienced the mobilization of its shear strength soon after the maximum horizontal displacement and started exhibiting the traces of cyclic mobility (accumulation of horizontal displacement in one direction) after t = 28 s. However, the ground with granular column did not show such a tendency, and the residual horizontal displacement is marginal in comparison with the ground without a granular column.

3.2 Evolution of excess pore water pressure

The evolution of excess pore water pressure (EPWP) plays a vital role in the manifestation of liquefaction during the dynamic event. Figure 6 shows the EPWP generation and dissipation trends at different depths along a selected point C (see Figure 2) for the grounds with and without a granular column. The soil at certain depth undergoes liquefaction state if the excess pore water pressure ratio (r_u), which is the ratio of EPWP and the initial vertical effective stress at respective depth, approaches one. During the early phase of shaking, the generation rate of EPWP is typical for both the grounds. However, the ground without granular column shows a significantly larger magnitude of maximum EPWP, even approaching $r_u = 1$ line (liquefaction state) at depths Z = 5, 8, and 10 m. The ground with granular column exhibits significantly faster dissipation of EPWP after t = 20 s in comparison with the ground without the granular column. The observed trends signify that the presence of a granular column is able to restrict the evolution of EPWP to minimize the extent of the liquefaction in the ground.

Contours of maximum r_u for the grounds with and without granular column at different depths are shown in Figure 7. Four different planes are selected at different depths Z = 2.25, 4.25, 6.25 and 8.25 m (depths are selected below the water table or drainage boundary to examine the apparent effects of granular column). Figure 7(a) depicts that the ground without granular column undergoes liquefaction as the values of r_u is in the range of 0.90 – 1.0 for all the planes at depths Z = 2.25, 4.25, 6.25, and 8.25 m

(however, slightly lower values of r_u in the range of 0.85 – 0.90 are observed for a few elements at depth Z = 2.25 m). The presence of granular column is found to restrict the evolution of EPWP remarkably as the r_u values are significantly lower for the ground with the granular column in caparison with the ground without granular column as depicted in Figure 7(b). The best performance of the granular column appeared to be just below the base of the granular column (at depth Z = 6.25 m, noted that the depth of the granular column is 6 m). The base of the granular column acts as a drainage boundary for the pore fluid during the earthquake. The strong hydraulic gradients steer the pore fluid toward the granular column, which facilitates in the significant dissipation of EPWP (Kumar et al. 2019b). This also corroborates the observation that the granular column is able to restrict the values of r_u in the range of 0.70 – 0.85 for a plane at a depth Z = 8.25 m, which is significantly deeper from the base of the granular column.

3.3 Shear reinforcement

The deformed shapes (10 times magnified) after the shaking and the distribution of excess pore water pressure ratio (r_u) at t = 16 s for the grounds with and without granular column are shown in Figure 8. It is evident from Figure 8(a) that the ground without the granular column undergoes significant deformation (both settlement and horizontal displacement). The ground exhibited mobilization of shear strength for depths Z = 4 - 6 m (element behavior at Z =5 m is shown in Figure 9(a)). The ground also exhibited the state of liquefaction ($r_u \sim 1$, for depths Z = 3 – 9 m, as shown in Figure 8(b)). The liquefaction in the ground resulted in the mobilization of shear strength during the shaking, which lead to the excessive deformation of the ground. The presence of granular column increased the overall stiffness of the ground (discussed later with Figures 9 and 10) and minimized the overall liquefaction extent of the ground (Figures 7 and 8(b)), which restricted the deformation of the ground.

Stress-strain curves for elements of array E, at Z = 5 and 10 m (see Figure 2) for the grounds with and without granular column are shown in Figure 9. It is evident from Figure 9(a) that the element of the ground without the granular column undergoes considerable shear strain in comparison with the ground with the granular column. This also corroborates the observation made earlier that the ground without granular column exhibited mobilization of excessive shear strength for depths Z = 4 - 6 m (as discussed with Figure 8(a)). The stress-strain curves for the element at Z = 10 m (Figure 9(b)) exhibits the trace of relatively large stiffness degradation during the shaking for the ground without the granular column in comparison with the ground with the granular column. This implies that the presence of a granular column increases the overall stiffness of the ground. Besides, the granular column helped to minimize the liquefaction extent (Figures 7 and 8(b)), which also resulted in stiffer behavior of the ground with the granular column.

The general notion that the presence of a granular column increases the overall stiffness of the ground (Baez 1995) is further examined with Figures 10 and 11. The induced cyclic stress ratio during the shaking is proportional to the shear stress reduction coefficient per the simplified procedure of Seed and Idriss (1971), as shown in equation 1.

$$\mathrm{CSR} = \frac{\tau_s}{\sigma'_v} = 0.65\left(\frac{a_{max}}{g}\right)\left(\frac{\sigma_v}{\sigma'_v}\right)\mathrm{rd} \quad (1)$$

Where, CSR = cyclic stress ratio; τ_s = cyclic shear stress; σ'_v and σ_v = effective and total vertical stress at a depth of interest, respectively; a_{max} = peak horizontal acceleration; rd = shear stress reduction coefficient. Larger is the stress reduction coefficient, larger the induced cyclic stress ratio during the shaking. The effect of the granular column on shear stress distribution within the ground is estimated using R_{rd}, which is defined in equation 2.

$$R_{rd} = \frac{rd_{wg}}{rd_{ng}} \quad (2)$$

Where, rd_{wg} and rd_{ng} = shear stress reduction coefficient for the grounds with and without granular column, respectively. The value of R_{rd} can provide an insight into the shear reinforcement in the ground due to the granular column. For instance, the value of R_{rd} less than one, equal to one, and more than one implies that the ground with granular column experience proportionally smaller, equal, and larger shear stress, respectively, in comparison with the ground without the granular column.

Figure 10 shows the contours of R_{rd} at different depths (at the middle of the elements for planes Z = 0.25, 2.25, 4.25, 6.25 and 8.25 m) of the ground. The values of R_{rd} inside the zone of the granular column (see Figure 2) is more than or equal to one for planes Z = 0.25, 2.25, and 4.25 m as expected. This is associated with the fact that the granular column attracts larger shear stress due to its stiffer characteristics. The substantial spatial variation in the values of R_{rd} is evident at the top surface of the ground (plane Z = 0.25 m), which is associated with the deformation pattern. Besides, the load from the foundation-structure system is modeled as surface pressure (applied at the top surface of the ground), which also resulted in the attraction of significant shear stress due to the apparent inertial interaction during the dynamic loading. The values of R_{rd} for planes Z = 2.25 and 4.25 m are significantly less than one in the ground away from the zone of the granular column, which shows the substantial contribution in the shear reinforcement due to the presence of the granular column. A relatively uniform distribution of R_{rd} is observed for the planes Z = 6.25 and 8.25 m, and the values of R_{rd} are less than one. It is to be noted that the granular column is up to 6 m of depth (see Figure 2); however, the presence of the granular column seems to reduce the shear stress in the whole ground.

The presence of a granular column reduces the induced shear stress in the ground, as shown in Figure 10. However, the magnitude of shear strain in the ground may not

adhere to the shear reinforcement during the shaking. Figure 11 shows the contours of the ratio of shear strain (γ) at different depths (at the middle of the elements for planes Z = 0.25, 2.25, 4.25, 6.25 and 8.25 m) of the ground. The value of γ less than one signifies the contribution of shear reinforcement in reducing the shear strain in the ground due to the granular column. The strong spatial variation in the values of γ (values being close to one) is evident for the planes at depth Z = 0.25 and 2.25 m. This incompatibility in shear strain reduction is attributed to the complex deformation mechanism as reported by several researchers (Goughnour and Pestana 1998, Green et al. 2008, Olgun and Martin 2008, and Raymajhi et al. 2014) and should be taken into account while designing the gravel drainage system.

4. Stochastic analyses

4.1 Numerical model

The nonuniformity of the ground is mapped using the overburden and energy-corrected, equivalent clean sand, SPT $(N1)_{60cs}$ values. For a given $(N1)_{60cs}$ value, the relative density (D_R) is calculated per equation 3 (Boulanger and Ziotopoulou, 2017).

$$D_R = \sqrt{\frac{(N1)_{60cs}}{46}} \quad (3)$$

A Gaussian correlation function is used, and the random field is generated with Karhunen Loeve (KL) decomposition method (Constantine and Wang, 2012, 2020). The discretized mesh (Figure 2) is implemented in the matrix form of size n by d; where n is the number of nodes and d is the dimension of the random field. The coefficient of variation (COV = 40%) and scale of fluctuation (θx = 5.0 m and θz = 0.5 m) are considered to model the nonuniformity of the ground according to Phoon and Kulhawy (1999) and Montgomery and Boulanger (2016). The nonuniformity of the ground is modeled with a mean $(N1)_{60cs}$ = 12 (D_R ~ 50%), as shown in Figure 12. A series of three-dimensional stochastic dynamic

304 analyses are performed considering the nonuniformity of the ground using anisotropic,
305 spatially correlated Gaussian random fields of $(N1)_{60cs}$ values. The parameters of
306 PDMY02 are calibrated for a wide range of relative densities corresponding to $(N1)_{60cs}$
307 of 5 ($D_R \sim 32\%$) to $(N1)_{60cs}$ of 26 ($D_R \sim 75\%$). The parameters of the PDMY02 Model are
308 calibrated to achieve the single-amplitude shear strain of 3% in cyclic undrained simple
309 shear loading with zero initial static shear stress ratio on a horizontal plane at a single
310 element level as described earlier. The target strength (CRR for 3% single-amplitude
311 shear strain in 15 uniform cycles) for different relative densities are estimated using the
312 SPT-based correlation as suggested by Boulanger and Idriss (2014). Numerically
313 simulated CSR curves for relative densities of $D_R = 30$ and 75% are compared with the
314 CSR curves obtained in the experiment (after Tatsuoka et al. 1982; and Tsukamoto et al.
315 2006), as shown in Figure 13 (CSR curves for $D_R = 50\%$ is shown in Figure 3(d)). Figures
316 3(d) and 13 exhibit that the calibrated parameters reasonably approximate the dynamic
317 behavior of Toyoura sand. The calibrated parameters for 17 different individual relative
318 densities ranging from $D_R = 30 – 75\%$ are tabulated in Table 3. For intermediate relative
319 densities, linear interpolation is used to get the calibrated parameters. The granular
320 column and associated ground (Toyoura Sand) is assigned a uniform permeability value
321 of 0.0066 and 0.0002 m/s, respectively. The assigned uniform properties for the granular
322 column is corresponding to $(N1)_{60cs}$ of 30 ($D_R \sim 80\%$), per Raymajhi et al. (2016) and
323 Khosravifar et al. (2018). The random field of $(N1)_{60cs}$ values with calibrated parameters
324 of the PDMY02 Model are implemented into the OpenSees numerical model with the
325 help of Matlab code.

326 Figure 14 shows the typical variation of the mean and standard deviation of the
327 average settlement and horizontal displacement of the top surface ($Z = 0$ plane, see Figure
328 2) of the ground with the granular column. The mean and standard deviation become
329 stable within fifty realizations, and hence, a reliable statistical interpretation of the

stochastic data can be obtained from the series of nonlinear dynamic numerical simulations. It should be noted that the larger the number of realizations, the better the reliability of the statistical interpretation. However, the numerical computational expense should be taken into account when selecting the total number of realizations without compromising with the stability of the mean and standard deviation of the primary stochastic outcomes (e.g., the average settlement and horizontal displacement of the top surface of the ground in this study).

4.2 Stochastic distribution of ground deformation

The results of three–dimensional stochastic analyses are presented and compared with the deterministic analysis results. Figure 15 illustrates the stochastic distribution of the average settlement and horizontal displacement of the top surface of the ground (Z = 0 plane, see Figure 2) for the grounds with and without a granular column. Figure 15(a) depicts that the mean (μ) and the standard deviation (σ) of the average surface settlement is 4.31 cm and 0.23 cm, respectively, for the ground with the granular column. It is observed that the mean of stochastic average surface settlement is significantly larger than the respective deterministic value. Whereas, the mean (μ) and the standard deviation (σ) of the average surface settlement is 4.80 cm and 0.10 cm, respectively, and the mean value is comparable to the deterministic value for the ground without the granular column. A relatively wider stochastic distribution and considerable standard deviation in the average surface settlement is evident in the case of the ground with the granular column in comparison with the ground without a granular column. This emphasizes that the presence of a granular column may adversely affect the uncertainty in the prediction of the average surface settlement due to the inherent ground nonuniformity (further discussed with Figure 16). Figure 15(b) depicts that the mean (μ) and the standard deviation (σ) of the horizontal surface displacement is 0.31 cm (distribution in the range of -1.0 cm to 1.5 cm)

355 and 0.60 cm, respectively, for the ground with the granular column. Whereas, the mean
356 (μ) and the standard deviation (σ) of the surface horizontal displacement is -3.17 cm
357 (distribution in the range of -6.0 cm to -1.0 cm) and 1.34 cm, respectively, for the ground
358 without granular column. The mean of the stochastic distribution is comparable with the
359 deterministic values for both the cases of grounds with and without the granular column.
360 However, a relatively wider stochastic distribution and considerable standard deviation
361 in the horizontal surface displacement is evident in the case of the ground without the
362 granular column in comparison with the ground with the granular column. This
363 emphasizes that the presence of a granular column may favorably affect the uncertainty
364 in the prediction of horizontal surface displacement (further discussed with Figure 16).
365 The reason for this is the shear reinforcement of the ground due to the stiffness of the
366 granular column, which is the governing factor for the residual amount of horizontal
367 surface displacement, as discussed earlier. Besides, the granular column is considered
368 with uniform properties (Table 1), which facilitated relatively less uncertainty in the
369 prediction of surface horizontal displacement in the case of the ground with the granular
370 column in comparison with the ground without a granular column.

371 The probability of deviation of the stochastic average settlement and horizontal
372 displacement of the top surface of the ground from their deterministic values are evaluated
373 and presented in Figure 16 for the grounds with and without the granular column. The
374 deviations of the average settlement and horizontal displacement of the top surface of the
375 ground are considered on the positive side (more than the deterministic value) and the
376 negative side (less than the deterministic value). Figure 16(a) shows that total
377 probabilities of the stochastic average surface settlement being deviated on the negative
378 side from the deterministic value are 13.07 and 40.03%, respectively, and on the positive
379 side from the deterministic value are 86.45 and 56.65%, respectively, for the grounds with
380 and without granular column. The maximum deviation of the average surface settlement

381 on the negative side is 0.20 cm (with a 2.32% probability of occurrence) and 0.29 cm
382 (with a 0.09% probability of occurrence), respectively, for the grounds with and without
383 granular column. The maximum deviation of the average surface settlement on the
384 positive side is 0.62 cm (with a 5.97% probability of occurrence) and 0.19 cm (with a
385 4.43% probability of occurrence), respectively, for the grounds with and without granular
386 column. A relatively larger deviation from the deterministic value associated with a
387 significant probability of occurrence in case of the ground with granular column signifies
388 that the presence of granular column adversely affects the uncertainty in the prediction of
389 the average surface settlement due to the inherent ground nonuniformity as discussed
390 earlier (with Figure 15(a)). Figure 16(b) shows that total probabilities of stochastic
391 surface horizontal displacement being deviated on the negative side from the
392 deterministic value are 57.05 and 42.68%, respectively, and on the positive side from the
393 deterministic value are 41.92 and 51.69%, respectively, for the grounds with and without
394 granular column. The maximum deviation of the horizontal surface displacement on the
395 negative side is 1.48 cm (with a 1.12% probability of occurrence) and 2.32 cm (with a
396 2.96% probability of occurrence), respectively, for the ground with and without granular
397 column. The maximum deviation of the horizontal surface displacement on the positive
398 side is 1.04 cm (with a 2.74% probability of occurrence) and 3.30 cm (with a 1.05%
399 probability of occurrence), respectively, for the grounds with and without granular
400 column. A relatively larger deviation from the deterministic value associated with a
401 significant probability of occurrence in the case of the ground without granular column
402 signifies that the presence of granular column favorably affects the uncertainty in the
403 prediction of the horizontal surface displacement due to the inherent ground
404 nonuniformity as discussed earlier (with Figure 15(b)).

405 ***4.3 Stochastic bounds of excess pore water pressure ratio***

406 Spatial nonuniformity is prone to influence the evolution of EPWP, which may
407 significantly affect the deformation mechanism of the ground (as witnessed in Figures 15
408 and 16). The efficacy of the granular column to restrict the r_u (for uniform ground, with
409 deterministic analyses) is discussed in Figure 7. Similarly, the contours of r_u at different
410 depths are estimated for each realization from the series of stochastic analyses considering
411 the spatial nonuniformity of the ground with the granular column to trace the worst
412 performance (the largest values of r_u) and best performance (smallest values of r_u) of the
413 granular column as shown in Figure 17. The contours of r_u in Figure 17(b) are
414 significantly larger than the contours of r_u shown in Figure 17(a), which implies that the
415 performance of granular column per the restriction of EPWP may be compromised due
416 to the nonuniformity of the ground. The values of r_u in Figures 7(b) (deterministic case)
417 and 17(b) (largest values of r_u based on stochastic analyses) signifies that the
418 nonuniformity in the ground prone to adversely affect the performance of the granular
419 column to restrict the r_u.

420 ***4.4 Stochastic surface spectral response spectrum***

421 The frequency and magnitude of the input shaking fluctuate (amplify or attenuate
422 depending upon the inertial and kinematic interaction) as the wave propagates toward the
423 surface of the ground (Kumar et al. 2019a). The presence of a granular column helps to
424 minimize the extent of liquefaction (Figure 7), which may affect the filtration of the high-
425 frequency content of the incident wave and the amplification in the magnitude of low-
426 frequency content of incident wave. For each realization, the displacement time history
427 of the top surface of the ground is recorded during the shaking. The spectral horizontal
428 displacement is calculated for a wide range of periods (T = 0.0005 ~ 4 s), considering a
429 damping ratio of 5%. Figure 18(a) shows the upper and lower bounds of surface spectral
430 horizontal displacement in comparison with the one for applied Tokachi-Oki ground

motion at the base. The stochastic bound of surface spectral horizontal displacement of the top surface of the ground is significantly larger than the corresponding values for Tokachi-Oki ground motion for a wide range of the periods (0.55 ~ 3.0 s). The probability of deviation of stochastic spectral horizontal displacement (for a different range of periods) from the corresponding values for Tokachi-Oki ground motion is evaluated and shown in Figure 18(b). The total probabilities of stochastic spectral displacement being more than the deterministic value are found in the range of 88.43 to 99.08% for structure periods 0.5 – 3.0 s. The maximum deviation in the spectral displacement from deterministic value is found in the range of 0.59 cm (with 2.68% probability of occurrence) to 1.31 cm (with 7.74% probability of occurrence) for structure periods 0.5 – 3.0 s. This wide range of deviation in spectral displacement from their deterministic values emphasizes that the nonuniformity of the ground (traced with the presented stochastic analyses) is vital to consider for a better insight of the surface response spectrum.

4.5 Effects of different ground motions

Kinematic and inertial interaction between soil and the granular column plays a vital role in the manifestation of the overall deformation of the ground during the dynamic event. The frequency and magnitude of the input shaking fluctuate as the wave propagates toward the surface of the ground. This alteration significantly depends on the anisotropic conditions resulted due to spatial nonuniformity, relative stiffness, the extent of liquefaction, and deformation pattern of the ground during the dynamic excitation. Each earthquake ground motion possesses a unique signature of frequency content, peak acceleration (PA), cumulative absolute velocity, Arias Intensity, and time duration. The results associated with Tokachi-Oki ground motion (discussed so far) may not necessarily represent the overall scenario of the performance of the granular column. Ten different

456 ground motions (GM1-GM10, see Table 4) are selected from the Pacific Earthquake
457 Engineering Research (PEER) using the procedure by Jayaram et al. (2011). The ground
458 motions possess a broad spectrum of frequency content and PA of interest, per Raymajhi
459 et al. (2016). The response spectra (damping 5%) for Tokachi-Oki and ten selected ground
460 motions along with their median are shown in Figure 19.

461 Selected ten ground motions are scaled for PA = 0.2, 0.4, and 0.6g. The ground
462 motions possess cumulative absolute velocity (CAV) and Arias Intensity (AI) in the range
463 of 2.3 – 34 m/s and 0.2 – 10.5 m/s, respectively. Deterministic analyses (Toyoura sand
464 with D_R = 50%) are carried out for these scaled ground motions to examine the fluctuation
465 in the average settlement and horizontal displacement of the top surface of the ground
466 with the granular column in comparison with the Tokachi-Oki ground motion. Figure
467 20(a) shows that the deterministic average surface settlement for Tokachi-Oki ground
468 motion (= 4.05 cm) is larger than the average surface settlement for all ten ground motions
469 (GM1-GM10) of PA = 0.2g. Similar trends are observed for eight ground motions of PA
470 = 0.4 and 0.6g except for two ground motions with the larger deterministic average
471 surface settlement than Tokachi-Oki ground motion. However, a significant deviation in
472 the horizontal surface displacement is observed for several selected ground motions from
473 the corresponding value for Tokachi-Oki ground motion (= 0.32 cm), as shown in Figure
474 20(b). The average surface settlement is found to be better correlated with the CAV and
475 AI than the PA of selected ground motions. Figure 20(a) depicts a strong correlation
476 between CAV, AI and average surface settlement. However, horizontal surface
477 displacement is found to be better correlated with the PA than CAV and AI of selected
478 ground motions as depicted in Figure 20(b). The horizontal surface displacement
479 primarily governed by the overall stiffness of the ground (as discussed with Figures 8 and
480 9), and thus large PA of the ground motion may adversely affect the stiffness degradation
481 of the granular column during the dynamic event. These statistics signify that a wide

spectrum of, PA, CAV, and AI of the ground motion is important to consider for a reliable estimate of the ground deformation.

Stochastic analyses are carried out for all the ground motions GM1-GM10 with PA = 0.6g, and the probabilities of deviation from the deterministic values of average settlement and horizontal displacement of the top surface of the ground are evaluated as shown in Figure 21. The interpretation is made in comparison with the respective probability of deviations for Tokachi-Oki ground motion (as reported in Figure 16). Figure 21(a) shows the probability of deviation of the average surface settlement from the deterministic values. It is evident that the deviation in the average surface settlement and probabilities of exceedance (especially on the positive side) are significantly exceeding the values traced with the Tokachi-Oki ground motion for several ground motions. Figure 21(b) shows the probability of deviation of the horizontal surface displacement from the deterministic values. It is evident that the deviation in the horizontal surface displacement for several ground motions are significantly exceeding the values traced with the Tokachi-Oki ground motion. Besides, the probabilities of exceedance for several ground motions are significantly larger for the deviations in both the positive and negative sides. This observation corroborates the fact that the characteristics of the ground motion (CAV, AI and PA) prone to significantly affect the effectiveness of granular column to mitigate the liquefaction-induced ground deformation.

5. Conclusions

A reliability assessment of the performance of equally-spaced granular columns in a nonuniform liquefiable ground is carried out to mitigate the liquefaction-induced ground deformation using three-dimensional (3D) stochastic numerical analyses. The PDMY02 elastoplastic soil constitutive model is used to simulate the dynamic behavior of the liquefiable ground treated with the granular column. The nonuniformity in the ground is

mapped with the stochastic realizations of the overburden and energy-corrected, equivalent clean sand, SPT $(N1)_{60cs}$ values using a spatially correlated Gaussian random field. It is found that the presence of a granular column increases the overall stiffness and minimizes the liquefaction extent of the ground. The favorable shear reinforcement within the ground is observed due to the granular column. However, incompatibility in shear strain reduction is also noted due to the complex deformation mechanism. The spatial nonuniformity in the ground is found to affect the liquefaction-induced ground deformation. Stochastic results depicted that the presence of the granular column reduces the uncertainty in the estimation of horizontal displacement; however, it adversely affects the uncertainty in the prediction of the average surface settlement of the ground. The stochastic displacement spectra exhibited that the nonuniformity of the ground should be taken into account, especially for long-period structures. Besides, the wide range of deviation in spectral displacement from their deterministic value emphasizes that the nonuniformity of the ground is important to consider for a better insight of the surface response spectrum. It is found that the characteristics of ground motions (CAV, AI, and PA) significantly affect the liquefaction-induced ground deformation. Stochastic results emphasize that the reliability assessment of the performance of the granular column is essential for better engineering judgment. The presented probabilistic assessment traces the conservative nature of the deterministic performance of granular column and possesses significant practical importance. The findings of shear reinforcement, strain incompatibility, probabilistic estimates of liquefaction-induced ground deformation, stochastic bound of the evolution of EPWP, and effects of different ground motions will assist in bridging the gap of risk information while designing the granular columns with conventional design charts. For a generalized framework to incorporate the reduction in the epistemic uncertainty, it is necessary to investigate further the full scenario of the gravel drainage system with the foundation-structure system and different ground

conditions.

Acknowledgments

The first author sincerely acknowledges the support provided by the Monbukagakusho (Ministry of Education, Culture, Sports, Science, and Technology) scholarship for international graduate students. The authors are also indebted to Dr. Gabriele Chiaro, Senior Lecturer, Department of Civil and Natural Resources Engineering, University of Canterbury, New Zealand, for sharing the results of his experiments.

References

Adalier, K., Elgamal, A., Meneses, J., and Baez, J. I. 2003. "Stone columns as liquefaction countermeasure in non-plastic silty soils." *Soil Dynamics and Earthquake Engineering* 23 (7): 571-584. https://doi.org/10.1016/S0267-7261(03)00070-8

Adalier, K., and Elgamal, A. 2004. "Mitigation of liquefaction and associated ground deformations by stone columns." *Engineering Geology* 72 (3): 275-291. https://doi.org/10.1016/j.enggeo.2003.11.001

Adamidis, O., Madabhushi, G. S. 2019. "Numerical modelling of post-liquefaction reconsolidation." *2nd International Conference on Natural Hazards & Infrastructure, Crete island, Greece,* Paper No. 963.

Baez, J. I. 1995. "A design model for the reduction of soil liquefaction by using vibro-stone columns." PhD thesis, University of southern California, USA.

Bouckovalas, G. D., Papadimitriou, A. G., Kondis, A., and Bakas, G. J. 2006. "Equivalent-uniform soil model for the seismic response analysis of sites improved with inclusions." In *Proc. 6th European Conference on Numerical Methods in Geotechnical Engineering*, Taylor & Francis, London, 801-807.

Boulanger, R. W., Idriss, I. M., Stewart, D. P., Hashash, Y., Schmidt, B. 1998. "Drainage capacity of stone columns or gravel drains for mitigating liquefaction." In *Proc. Geotechnical Earthquake Engineering and Soil Dynamics III,* 678-690.

Boulanger, R. W., and Idriss, I. M. 2014. "CPT and SPT based liquefaction triggering procedures." *Center for Geotechnical Modeling Report No. UCD/CGM-14/01*, Department of Civil and Environmental Engineering, University of California, Davis, Calif.

Boulanger, R. W., and Ziotopoulou, K. 2017. "PM4Sand (Version 3.1): A sand plasticity model for earthquake engineering applications." *Center for Geotechnical Modeling Report No. UCD/CGM-17/01*, Department of Civil and Environmental Engineering, University of California, Davis, Calif.

Brennan, A. J., and Madabhushi, S. P. G. 2002. "Effectiveness of vertical drains in mitigation of liquefaction". *Soil Dynamics and Earthquake Engineering* 22(9): 1059-1065. https://doi.org/10.1016/S0267-7261(02)00131-8.

Chiaro, G., Koseki, J., and Sato, T. 2012. "Effects of initial static shear on liquefaction and large deformation properties of loose saturated Toyoura sand in undrained cyclic torsional shear tests." *Soils and Foundations* 52 (3): 498-510. https://doi.org/10.1016/j.sandf.2012.05.008

Christian, J. T., Ladd, C. C., and Baecher, G. B. 1994. "Reliability applied to slope stability analysis." *Journal of Geotechnical Engineering* 120 (12): 2180-2207. https://doi.org/10.1061/(ASCE)0733-9410(1994)120:12(2180)

Dashti, S., and Bray, J. D. 2013. "Numerical simulation of building response on liquefiable sand." *Journal of Geotechnical and Geoenvironmental Engineering* 139 (8): 1235-1249. https://doi.org/10.1061/(ASCE)GT.1943-5606.0000853

Duncan, J. M. 2000. "Factors of safety and reliability in geotechnical engineering." *Journal of Geotechnical and Geoenvironmental Engineering* 126 (4): 307-316. https://doi.org/10.1061/(ASCE)1090-0241(2000)126:4(307)

Elgamal, A., Lu, J., and Forcellini, D. 2009. "Mitigation of Liquefaction-Induced Lateral Deformation in a Sloping Stratum: Three-dimensional Numerical Simulation." *Journal of Geotechnical and Geoenvironmental Engineering, ASCE* 35 (11): 1672-1682. https://doi.org/10.1061/(ASCE)GT.1943-5606.0000137

Goughnour, R. R., and Pestana, J. M. 1998. "Mechanical behavior of stone columns under seismic loading." In *Proc. 2nd Int. Conf. on Ground Improvement Techniques*, Singapore, 157-162.

Green, R. A., Olgun, C. G., and Wissmann, K. J. 2008. "Shear stress redistribution as a mechanism to mitigate the risk of liquefaction." *Geotechnical Earthquake Engineering and Soil Dynamics IV, Sacramento, California, May 18-22*.

Jayaram, N., Lin, T., and Baker, J. W. 2011. "A computationally efficient ground motion selection algorithm for matching a target response spectrum mean and variance." *Earthquake Spectra* 27(3): 797-815. https://doi.org/10.1193/1.3608002

Karimi, Z., and Dashti, S. 2015. "Numerical and centrifuge modeling of seismic soil–foundation–structure interaction on liquefiable ground." *Journal of Geotechnical and Geoenvironmental Engineering* 142 (1), 04015061. https://doi.org/10.1061/(ASCE)GT.1943-5606.0001346

Karimi, Z., and Dashti, S. 2016. "Seismic performance of shallow founded structures on liquefiable ground: validation of numerical simulations using centrifuge experiments." *Journal of Geotechnical and Geoenvironmental Engineering* 142 (6), 04016011. https://doi.org/10.1061/(ASCE)GT.1943-5606.0001479

Khosravifar, A., Elgamal, A., Lu, J., Li, J. 2018. "A 3D model for earthquake-induced liquefaction triggering and post-liquefaction response." *Soil Dynamics and Earthquake Engineering* 110: 43-52. https://doi.org/10.1016/j.soildyn.2018.04.008

Constantine P. G, Wang Q. 2012, 2020. “Random field simulation. <http://www.mathworks.com/matlabcentral/fileexchange/27613-random-field-simulation>.

Kumar, R., Horikoshi, K., and Takahashi, A. 2019a. “Centrifuge testing to investigate effects of partial saturation on the response of shallow foundation in liquefiable ground under strong sequential ground motions.” *Soil Dynamics and Earthquake Engineering* 125. https://doi.org/10.1016/j.soildyn.2019.105728

Kumar, R., Kasama, K., and Takahashi, A. 2020. “Reliability assessment of the physical modeling of liquefaction-induced effects on shallow foundations considering nonuniformity in the centrifuge model.” *Computers and Geotechnics* 122, 103558. https://doi.org/10.1016/j.compgeo.2020.103558

Kumar, R., Sawaishi, M., Horikoshi, K., and Takahashi, A. 2019b. “Centrifuge modeling of hybrid foundation to mitigate liquefaction-induced effects on shallow foundation resting on liquefiable ground.” *Soils and Foundations* 59 (6): 2083-2098. https://doi.org/10.1016/j.sandf.2019.11.002

Law, H. K., and Lam, I. P. 2001. “Application of periodic boundary for large pile group”. *Journal of Geotechnical and Geoenvironmental Engineering*, 127(10), 889-892. https://doi.org/10.1061/(ASCE)1090-0241(2001)127:10(889)

Montgomery, J., Boulanger, R. W. 2016. “Effects of spatial variability on liquefaction-induced settlement and lateral spreading.” J*ournal of Geotechnical and Geoenvironmental Engineering* 143 (1): 04016086. https://doi.org/10.1061/(ASCE)GT.1943-5606.0001584

Olarte, J., Paramasivam, B., Dashti, S., Liel, A., and Zannin, J. 2017. “Centrifuge modeling of mitigation-soil-foundation-structure interaction on liquefiable ground.” *Soil Dynamics and Earthquake Engineering* 97: 304-323. https://doi.org/10.1016/j.soildyn.2017.03.014

Olgun, C. G., and Martin, II, J. R. 2008. “Numerical modeling of the seismic response of columnar reinforced ground.” *Geotechnical Earthquake Engineering and Soil Dynamics IV, Sacramento, California, May 18-22*.

Phoon, K. K., and Ching, J. 2014. “Risk and reliability in geotechnical engineering.” Boca Raton, CRC Press.

Phoon, K. K., Kulhawy, F. H. 1999. “Characterization of geotechnical variability.” *Canadian Geotechnical Journal* 36 (4): 612-624. https://doi.org/10.1139/t99-038

Rayamajhi, D., Ashford, S. A., Boulanger, R. W., and Elgamal, A. 2016. “Dense granular columns in liquefiable ground. I: shear reinforcement and cyclic stress ratio

reduction." *Journal of Geotechnical and Geoenvironmental Engineering* 142 (7): 04016023. https://doi.org/10.1061/(ASCE)GT.1943-5606.0001474

Rayamajhi, D., Nguyen, T. V., Ashford, S. A., Boulanger, R. W., Lu, J., Elgamal, A., and Shao, L. 2014. "Numerical study of shear stress distribution for discrete columns in liquefiable soils." *Journal of Geotechnical and Geoenvironmental Engineering* 140 (3): 04013034. https://doi.org/10.1061/(ASCE)GT.1943-5606.0000970

Seed, H. B., and Booker, J. R. 1977. "Stabilization of potentially liquefiable sand deposits using gravel drains." *Journal of Geotechnical Engineering Division, ASCE* 103 (GT7): 757–768.

Seed, H. B., and Idriss, I. M. 1971. "Simplified procedure for evaluating the liquefaction potential." *Journal of Soil Mechanics and Foundation Division, ASCE* 97(SM9): 1249-1273.

Shahir, H., Pak, A., Taiebat, M., and Jeremić, B. 2012. "Evaluation of variation of permeability in liquefiable soil under earthquake loading." *Computers and Geotechnics* 40: 74-88. https://doi.org/10.1016/j.compgeo.2011.10.003

Stewart, J. P., Kwok, A. O., Hashash, Y. M. A., Matasovic, N., Pike, R., Wang, Z., and Yang, Z. 2008. "Benchmarking of nonlinear geotechnical ground response analysis procedures." *Pacific Earthquake Engineering Research Center Report No. 2008/04*, College of Engineering, University of California, Berkeley, Calif.

Taiebat, M., Shahir, H., and Pak, A. 2007. "Study of pore pressure variation during liquefaction using two constitutive models for sand." *Soil Dynamics and Earthquake Engineering* 27 (1), 60-72. https://doi.org/10.1016/j.soildyn.2006.03.004

Tatsuoka, F., Muramatsu, M., and Sasaki, T. 1988. "Cyclic undrained stress-strain behavior of dense sands by torsional simple shear test." *Soils and Foundations* 22 (2). https://doi.org/10.3208/sandf1972.22.2_55

Tokimatsu, K., Yoshimi, Y., Ariizumi, K. 1990. "Evaluation of liquefaction resistance of sand improved by deep vibratory compactions." *Soils and Foundation* 30 (3), 153–8. https://doi.org/10.3208/sandf1972.30.3_153

Tsukamoto, Y., Ishihara, K., Umeda, K., Enomoto, T. 2006. "Cyclic resistance of clean sand improved by silicate-based permeation grouting." *Soils and Foundations* 46 (2): 233-245. https://doi.org/10.3208/sandf.46.233

Yang, Z., Elgamal, A., Parra, E. J. 2003. "Computational Model for Cyclic Mobility and Associated Shear Deformation." *Geotechnical and Geoenvironmental Engineering,*

ASCE 129 (12): 1119-1127. https://doi.org/10.1061/(ASCE)1090-0241(2003)129:12(1119)

Tables

Table 1. Index properties of Toyoura sand and granular column

Description	Toyoura sand	Granular column (Silica no. 3)
Specific gravity, G_s	2.65	2.63
D_{50} (mm)	0.19	1.72
D_{10} (mm)	0.14	1.37
Maximum void ratio, e_{max}	0.973	1.009
Minimum void ratio, e_{min}	0.609	0.697
Permeability, k (m/s)	2.0E-4	6.6E-3

Table 2. Calibrated parameters for Toyoura sand and granular column

Material/Parameters*	ρ (ton/m^3)	G_{max} (kPa)	B (kPa)	φ	PT_{ang}	C1	C3	D1	D3
Toyoura sand (D_R = 50%)	1.94	3.54E4	7.50E4	33.5	25.5	0.07	0.20	0.06	0.20
Granular column (D_R = 80%)**	2.14	1.04E5	2.60E5	48.0	30.0	0.006	0.0	0.42	0.0

*Remaining parameters (total number of parameters are 22) received default values as reported by Khosravifar et al. (2018)

**The parameters for the granular column are selected per Elgamal et al. 2009, Raymajhi et al. 2016, and Khosravifar et al. (2018).

Table 3. Calibrated parameters for Toyoura sand with different relative densities (D_R = 30 - 75%)

D_R (%)	G_{max} (kPa)	B (kPa)	φ	PT_{ang}	C3	D1	D3
30	2.5E4	5.30E4	31.0	31.0	0.52	0.00	0.00
33	2.6E4	5.51E4	31.4	29.0	0.48	0.00	0.00
36	2.7E4	5.72E4	31.8	27.0	0.40	0.01	0.10
39	2.8E4	5.93E4	32.0	26.0	0.30	0.04	0.10
42	2.9E4	6.14E4	32.2	25.9	0.27	0.06	0.25
45	3.0E4	6.36E4	32.5	25.8	0.20	0.06	0.20
48	3.1E4	6.57E4	32.9	25.7	0.20	0.06	0.20
50	3.5E4	7.50E4	33.5	25.5	0.20	0.06	0.20
52	3.7E4	7.73E4	33.8	25.6	0.15	0.06	0.15
55	3.8E4	8.05E4	34.1	25.7	0.10	0.09	0.10
58	4.0E4	8.47E4	34.5	25.8	0.06	0.09	0.10
61	4.5E4	9.53E4	35.0	26.0	0.06	0.09	0.10
64	5.2E4	1.09E5	35.3	26.0	0.06	0.10	0.10
67	5.9E4	1.24E5	35.6	26.0	0.04	0.13	0.10
71	6.3E4	1.32E5	35.7	26.0	0.04	0.14	0.00
73	7.1E4	1.49E5	35.9	26.0	0.00	0.17	0.00
75	8.0E4	1.68E5	36.0	26.0	0.00	0.20	0.00

Note: C1 is 0.07 for all D_R. The remaining parameters (total number of parameters are 22) received default values as reported by Khosravifar et al. (2018)

Table 4. Earthquake ground motions (after Raymajhi et al. 2016)

Tag	Earthquake name	Year	Magnitude
GM1	Northridge 1	1994	6.69
GM2	Hector Mine 1	1999	7.13
GM3	Hector Mine 1	1999	7.13
GM4	Taiwan SMART 1	1986	7.3
GM5	Loma Prieta 1	1989	6.93
GM6	Northridge 2	1994	6.69
GM7	Alaska	2002	7.9
GM8	Loma Prieta 2	1989	6.93
GM9	Northridge 2	1994	6.69
GM10	Loma Prieta 3	1989	6.93

Figures

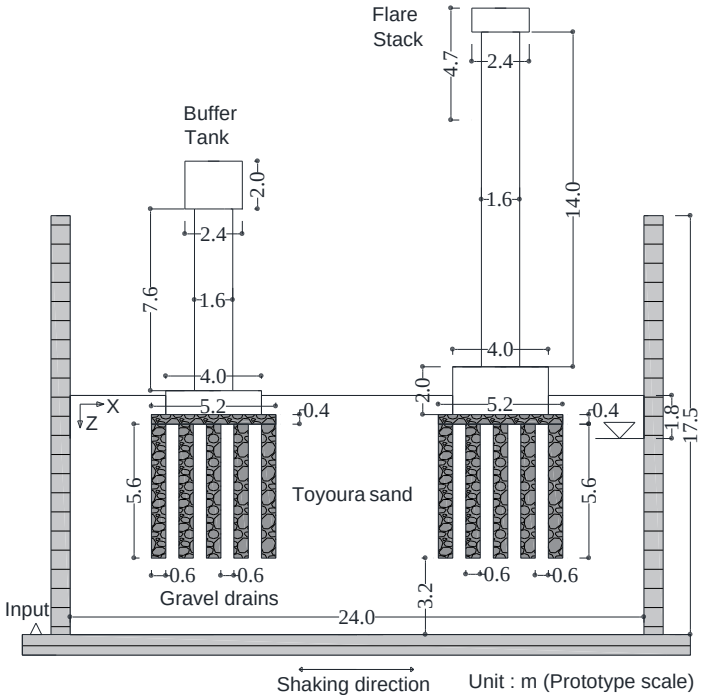

Figure 1. Centrifuge model configuration in the prototype scale

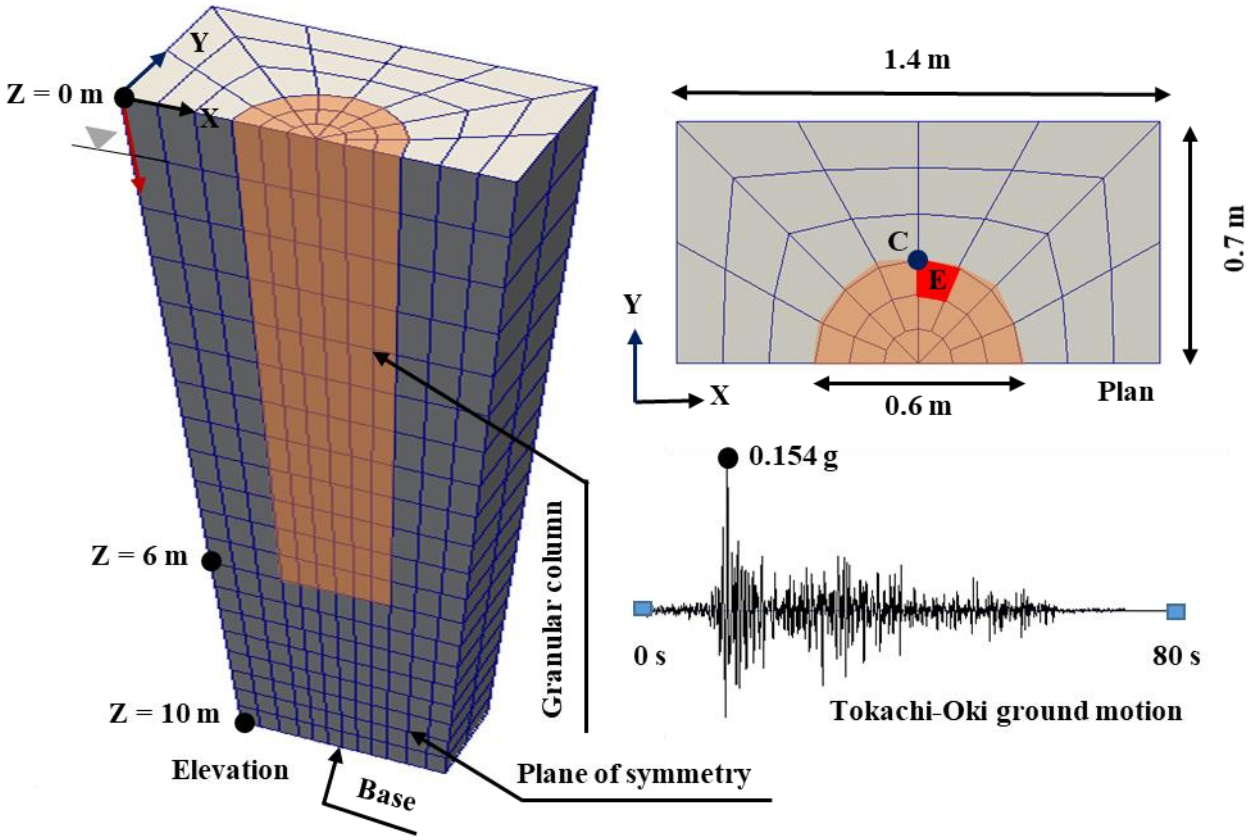

Figure 2. Three-dimensional (3D) numerical model

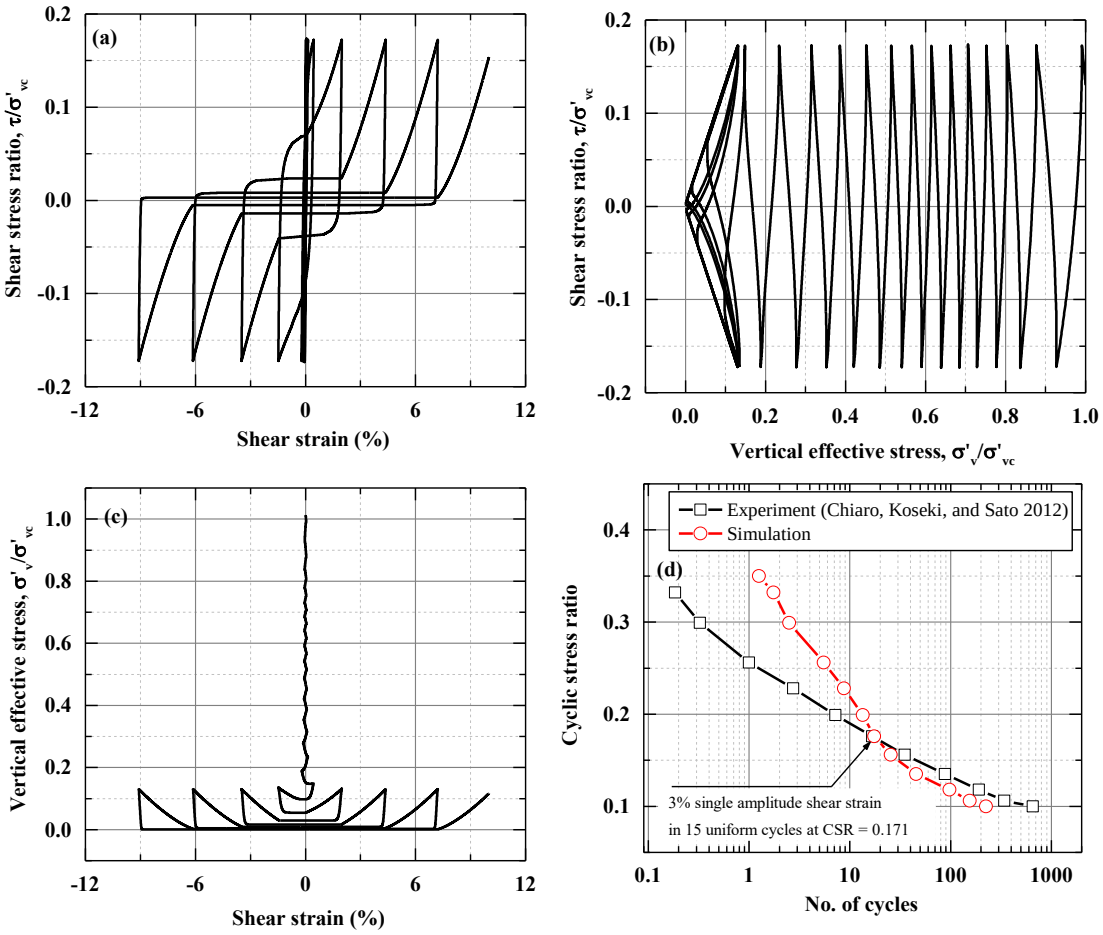

Figure 3. The response of the calibrated PDMY02 Model at the element level

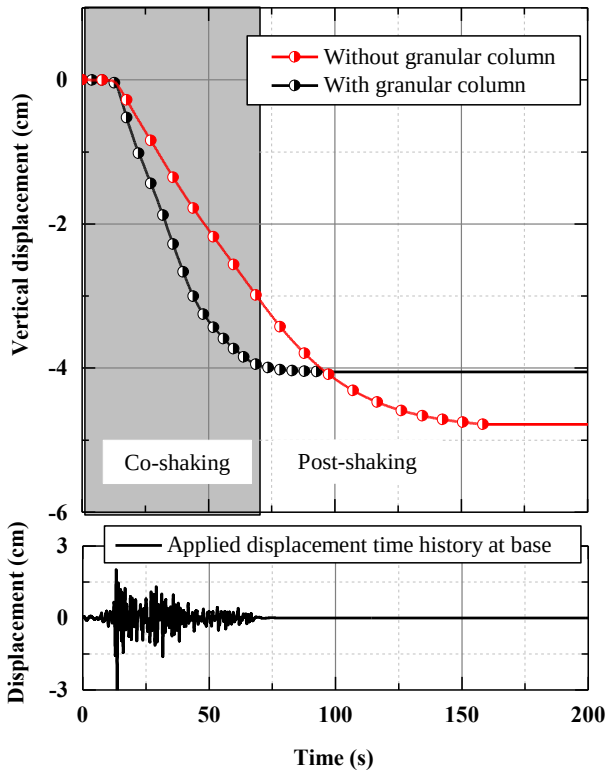

Figure 4. Average settlement of the top surface of the ground

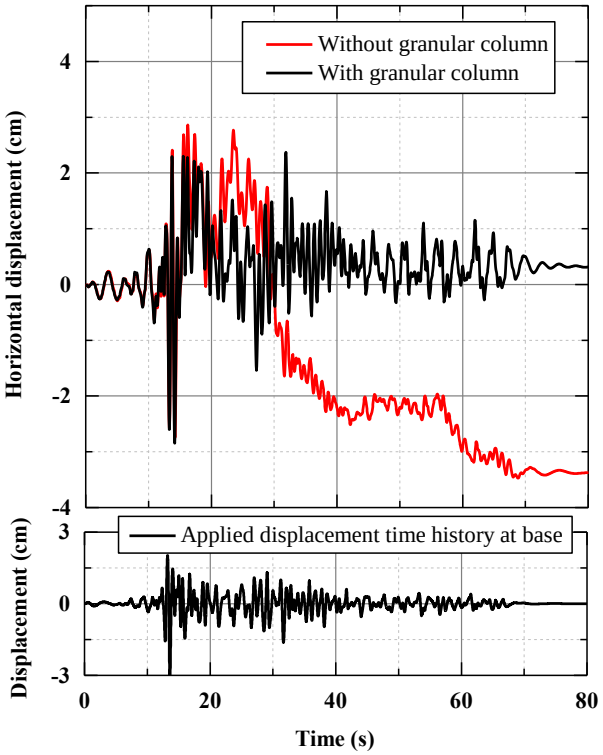

Figure 5. The horizontal displacement of the top surface of the ground

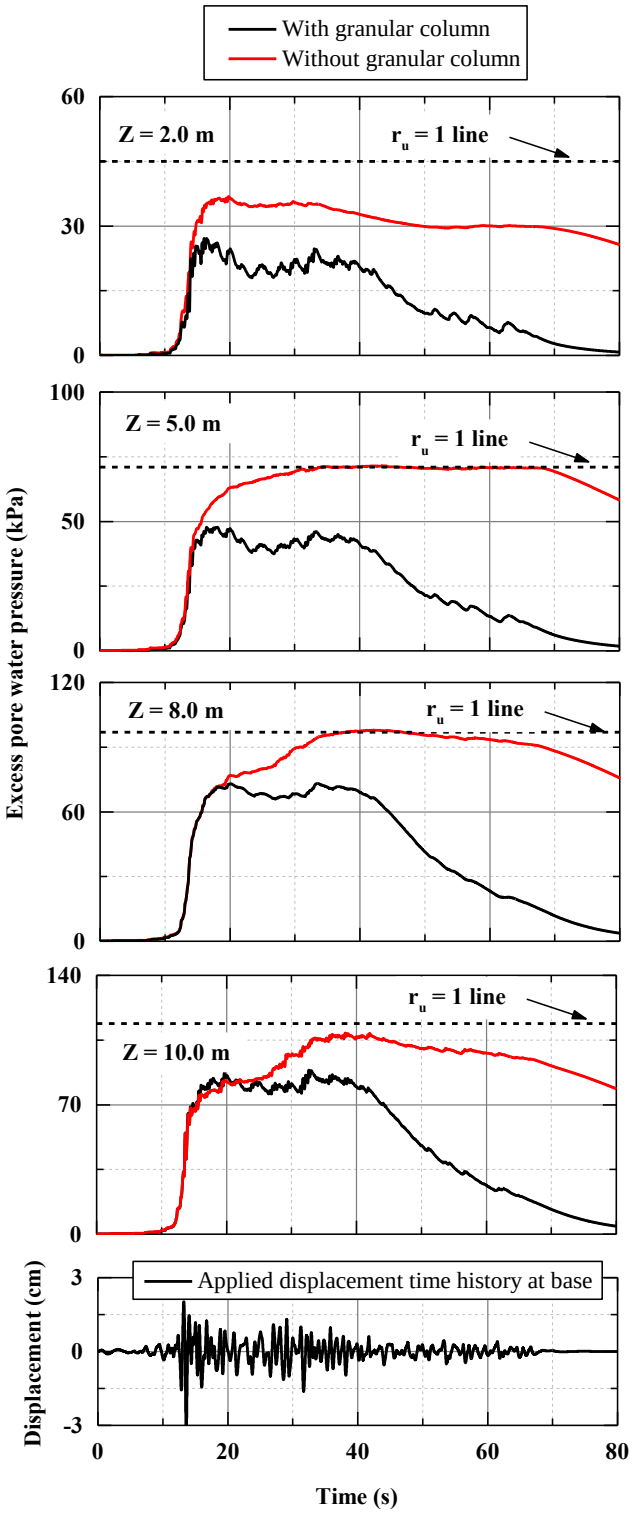

Figure 6. Evolution of excess pore water pressure along point C (see Fig. 2) at different depths for grounds with and without granular column

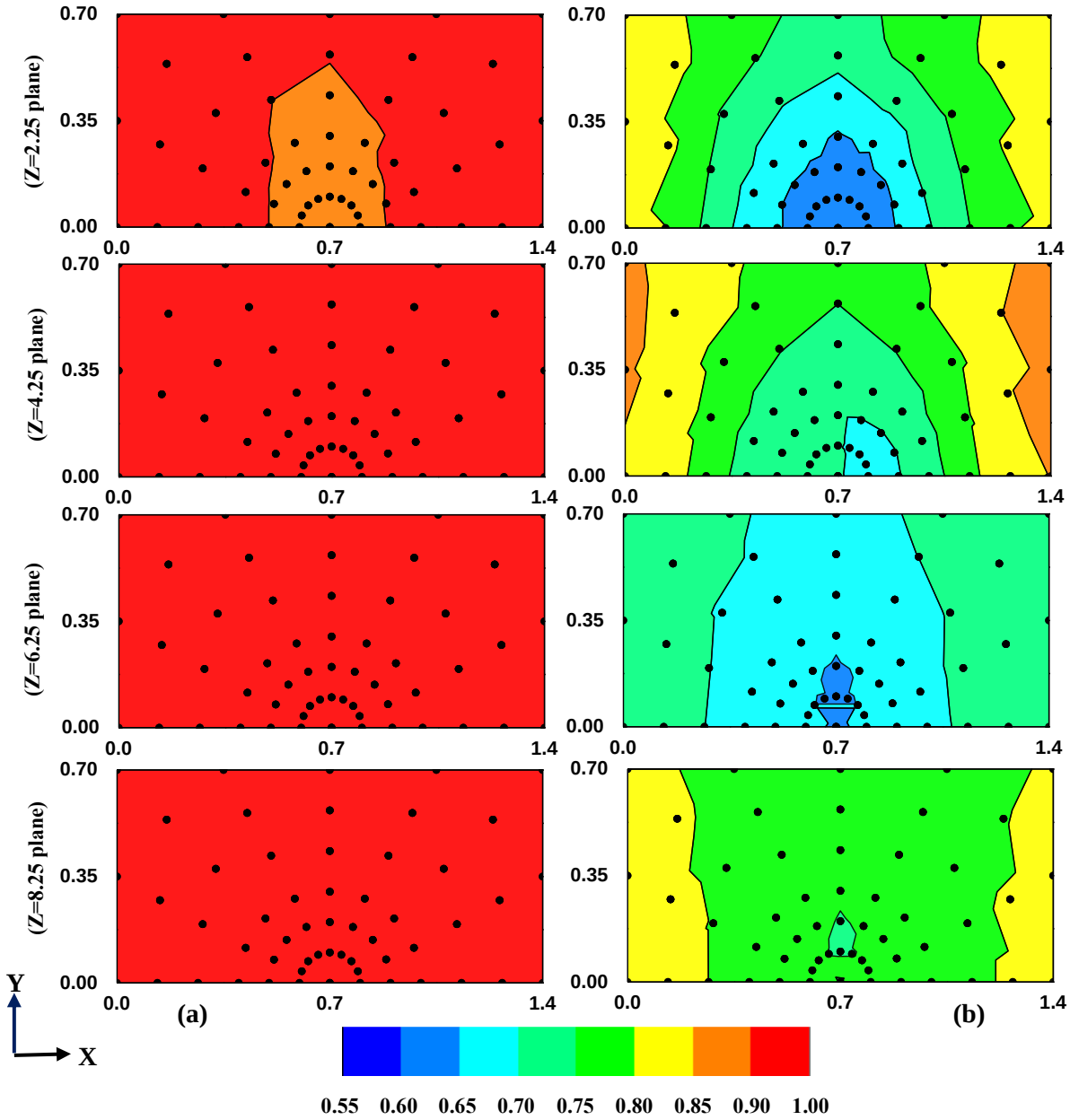

Figure 7. Contours of maximum r_u at different depths (planes Z = 2.25, 4.25, 6.25, and 8.25 m) for (a) ground without granular column and (b) ground with granular column

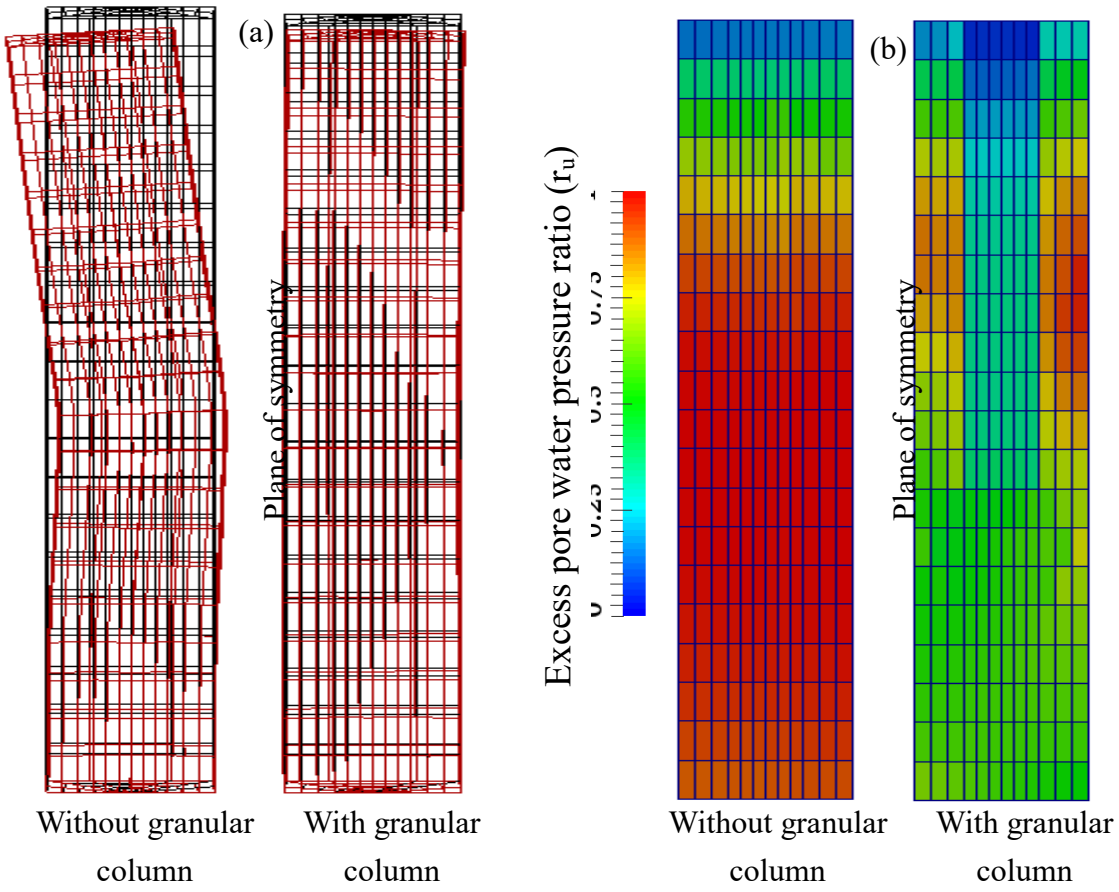

Figure 8. Ground response: (a) deformed shape (10 times magnified) after the shaking and (b) distribution of r_u at t = 16 s

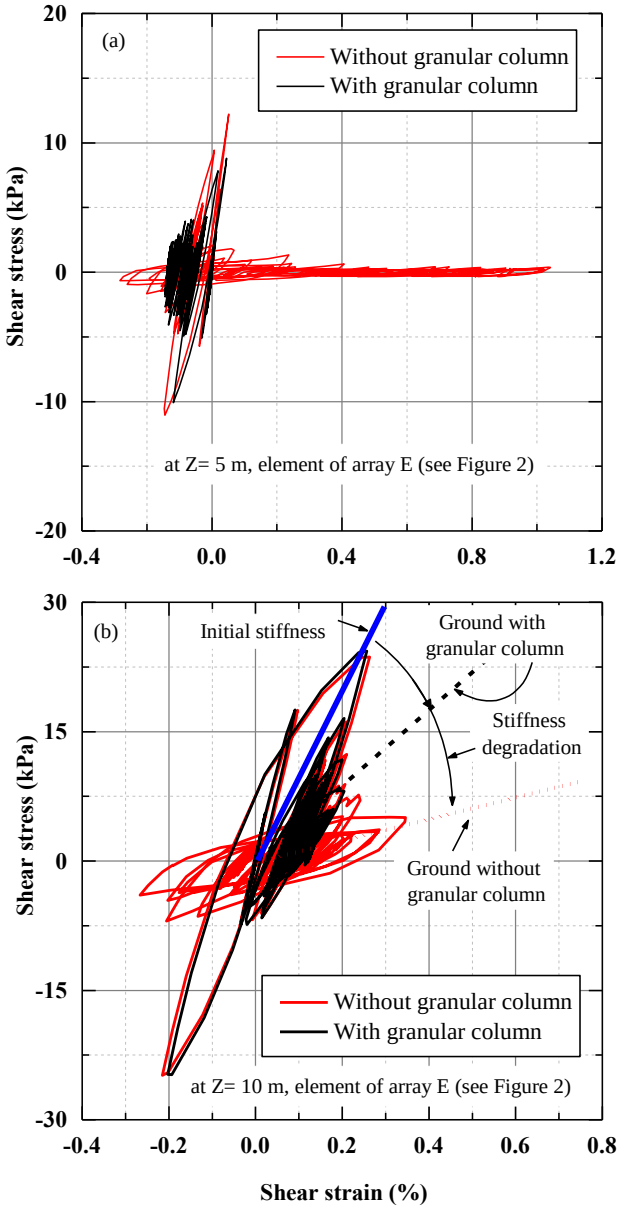

Figure 9. Typical stress-strain behavior for elements along E (see Fig. 2): (a) at depth Z = 5 m and (b) at depth Z = 10 m

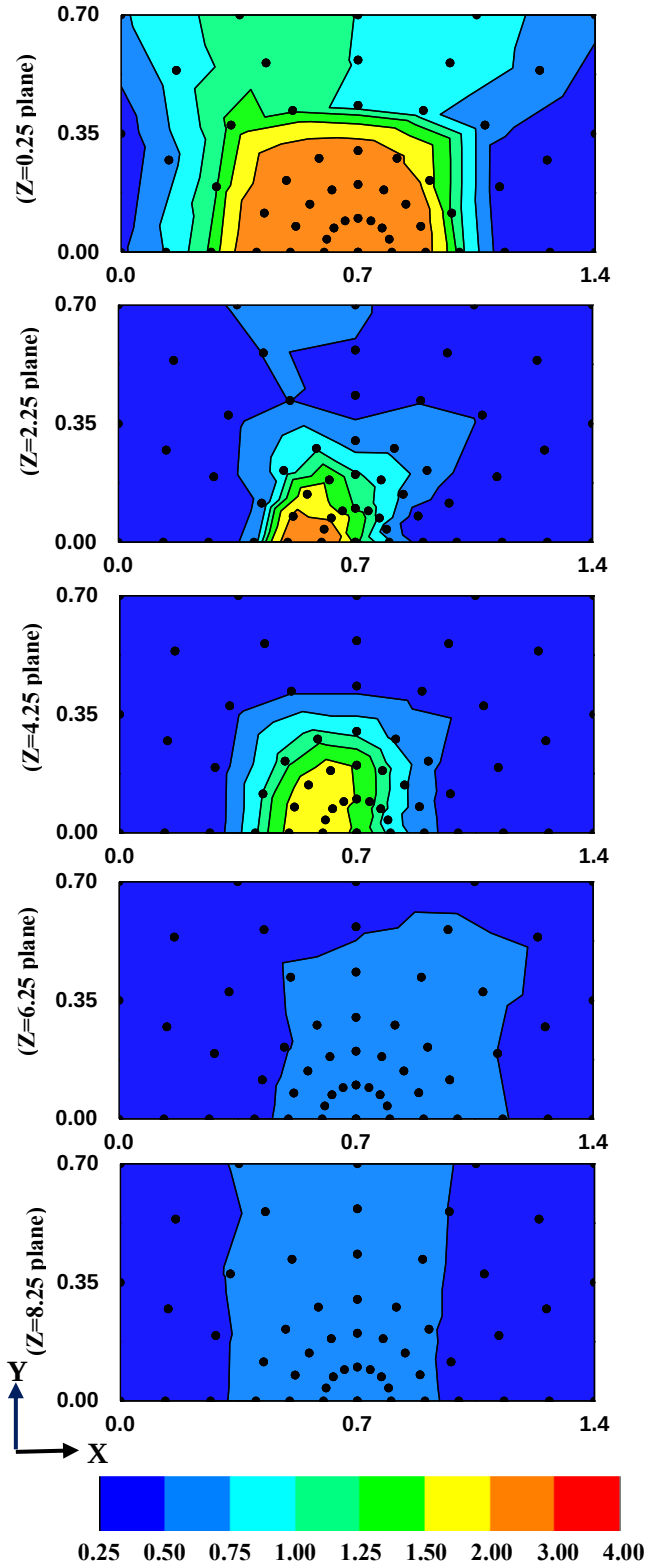

Figure 10. Contours of the ratio of maximum shear stress reduction coefficient (R_{rd}) at different depths (planes Z = 0.25, 2.25, 4.25, 6.25, and 8.25 m) of the ground

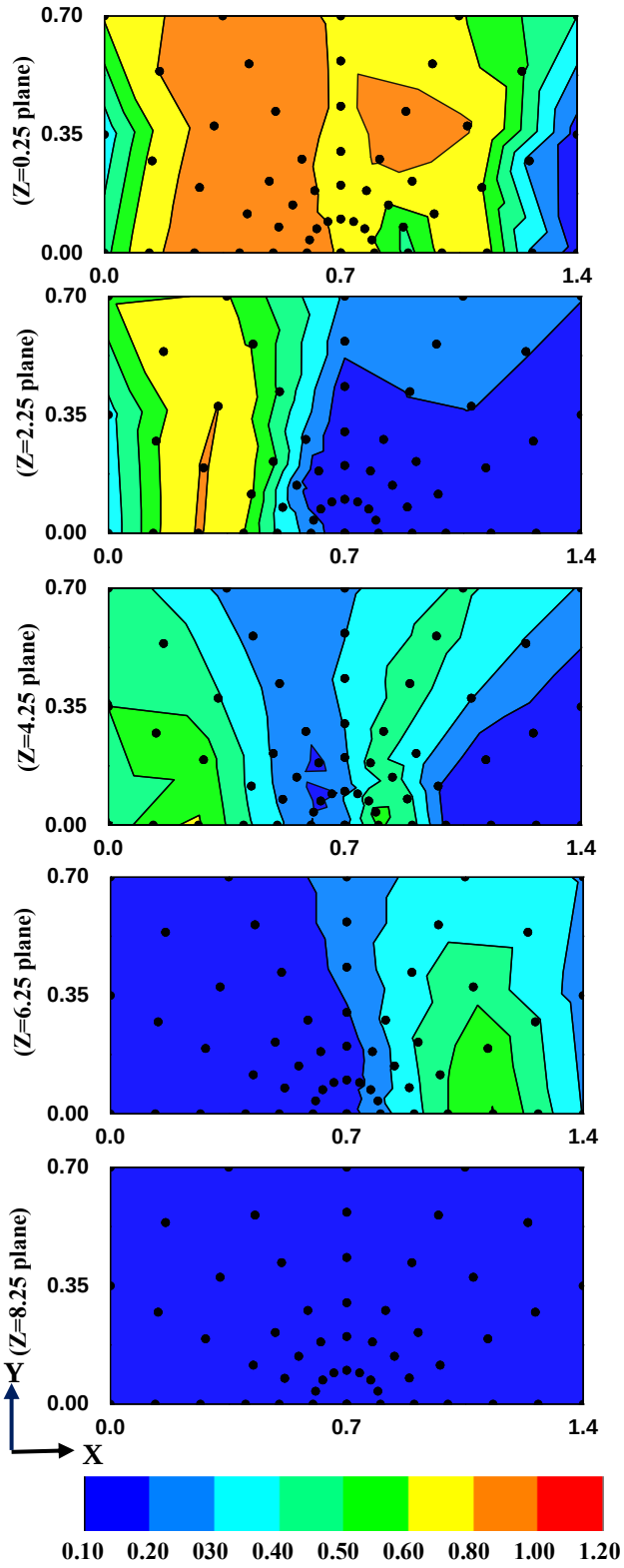

Figure 11. Contours of the ratio of maximum shear strain at different depths (planes Z = 0.25, 2.25, 4.25, 6.25, and 8.25 m) of the ground

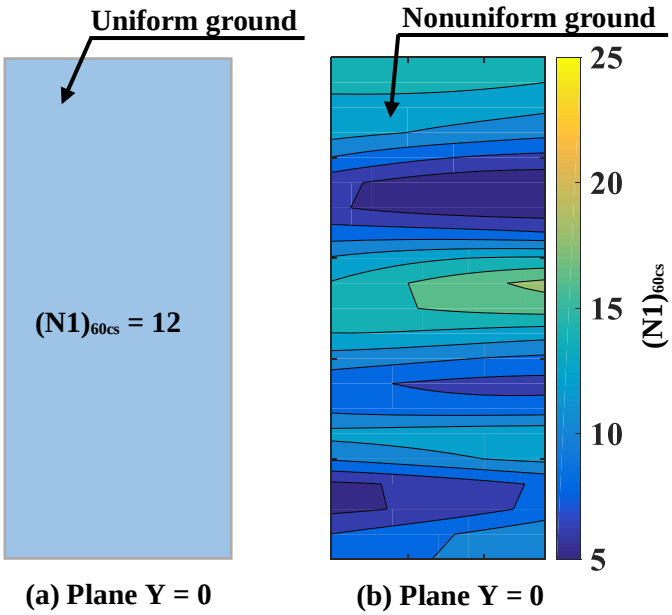

Figure 12. A typical scenario of the ground condition at Plane Y= 0 (see Figure 2): (a) uniform ground and (b) nonuniform ground

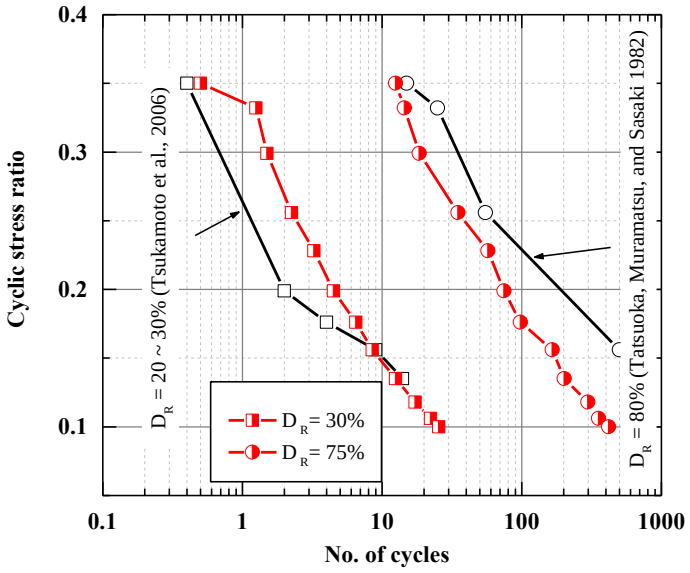

Figure 13. The response of the calibrated PDMY02 Model at element level for loose (D_R = 30%) and dense sand (D_R = 75%)

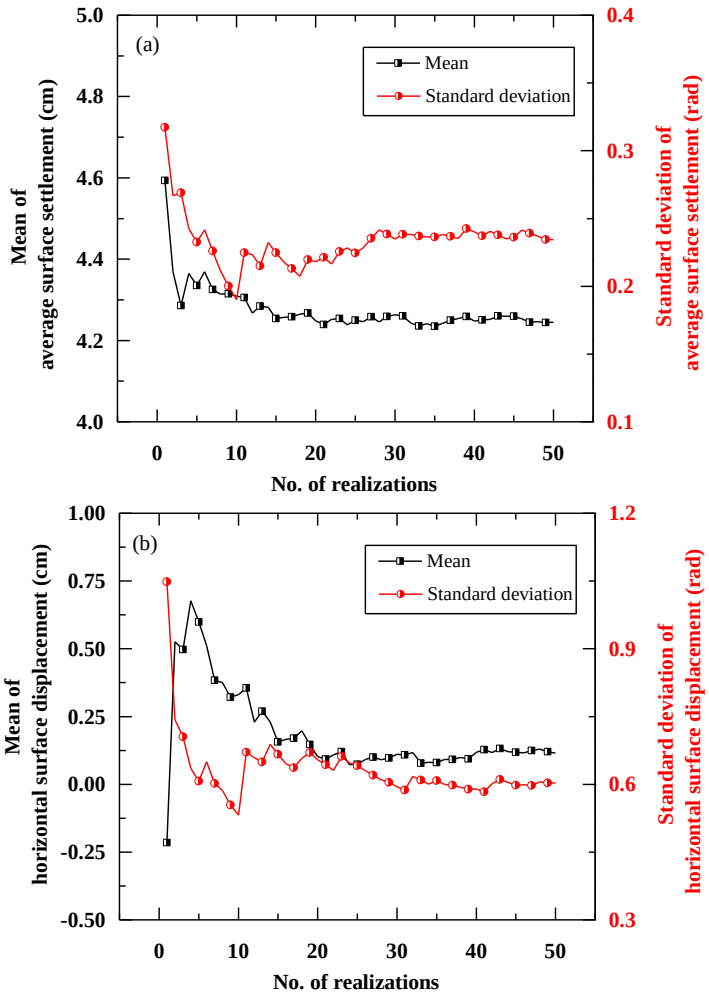

Figure 14. Convergence check for sufficient number of stochastic realizations

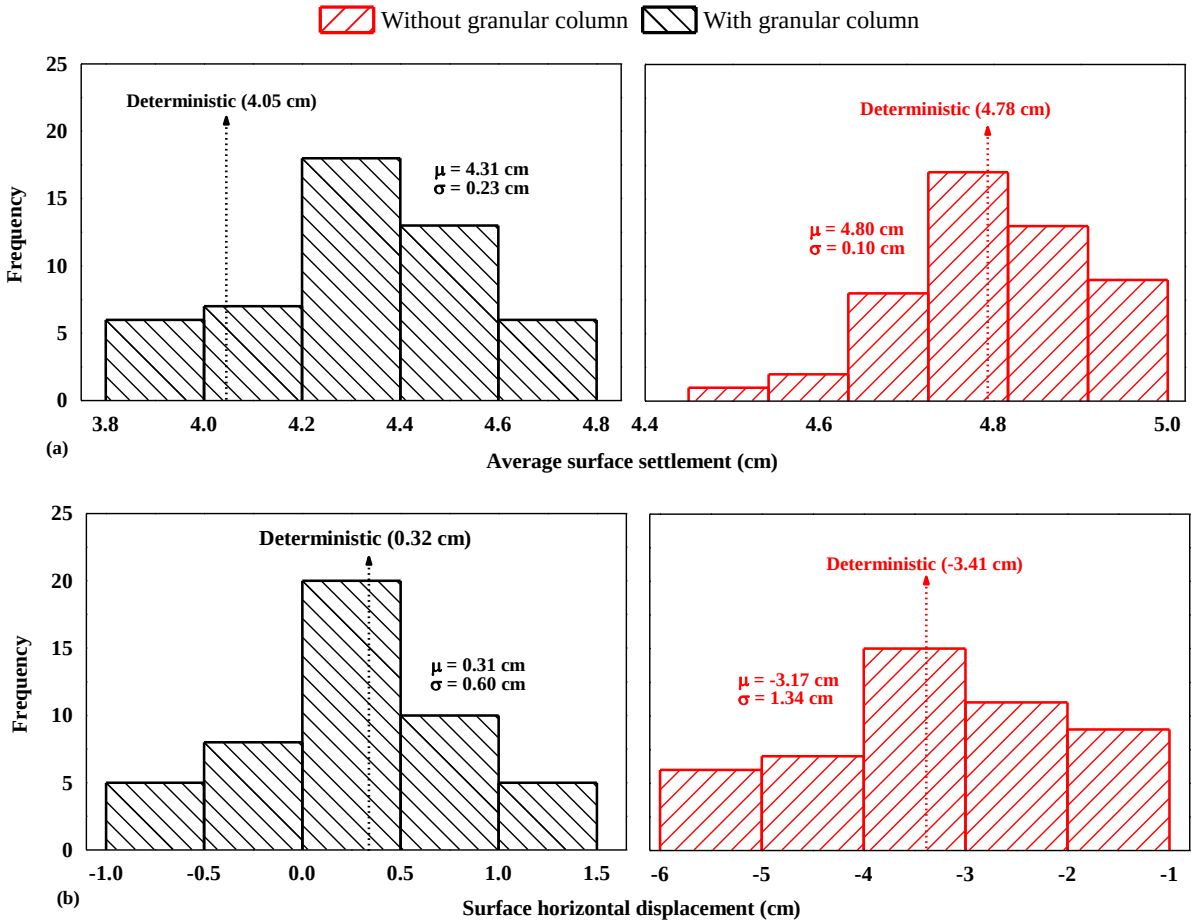

Figure 15. Stochastic distribution of model ground deformation for the grounds with and without granular column: (a) average surface settlement and (b) surface horizontal displacement

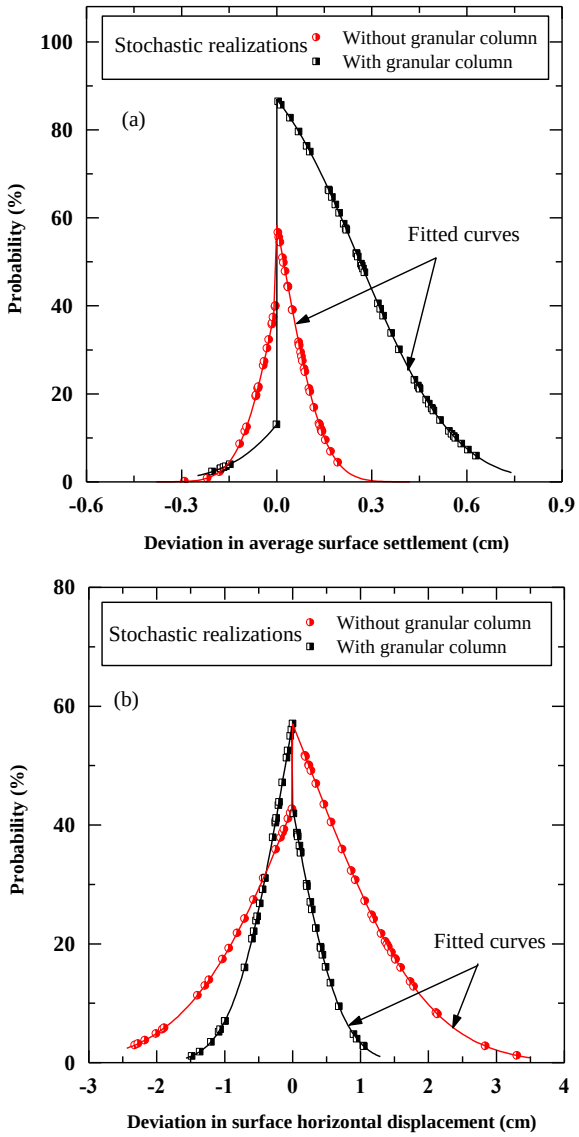

Figure 16. Probability of deviation from the deterministic values for the grounds with and without granular column: (a) for average surface settlement and (b) for surface horizontal displacement

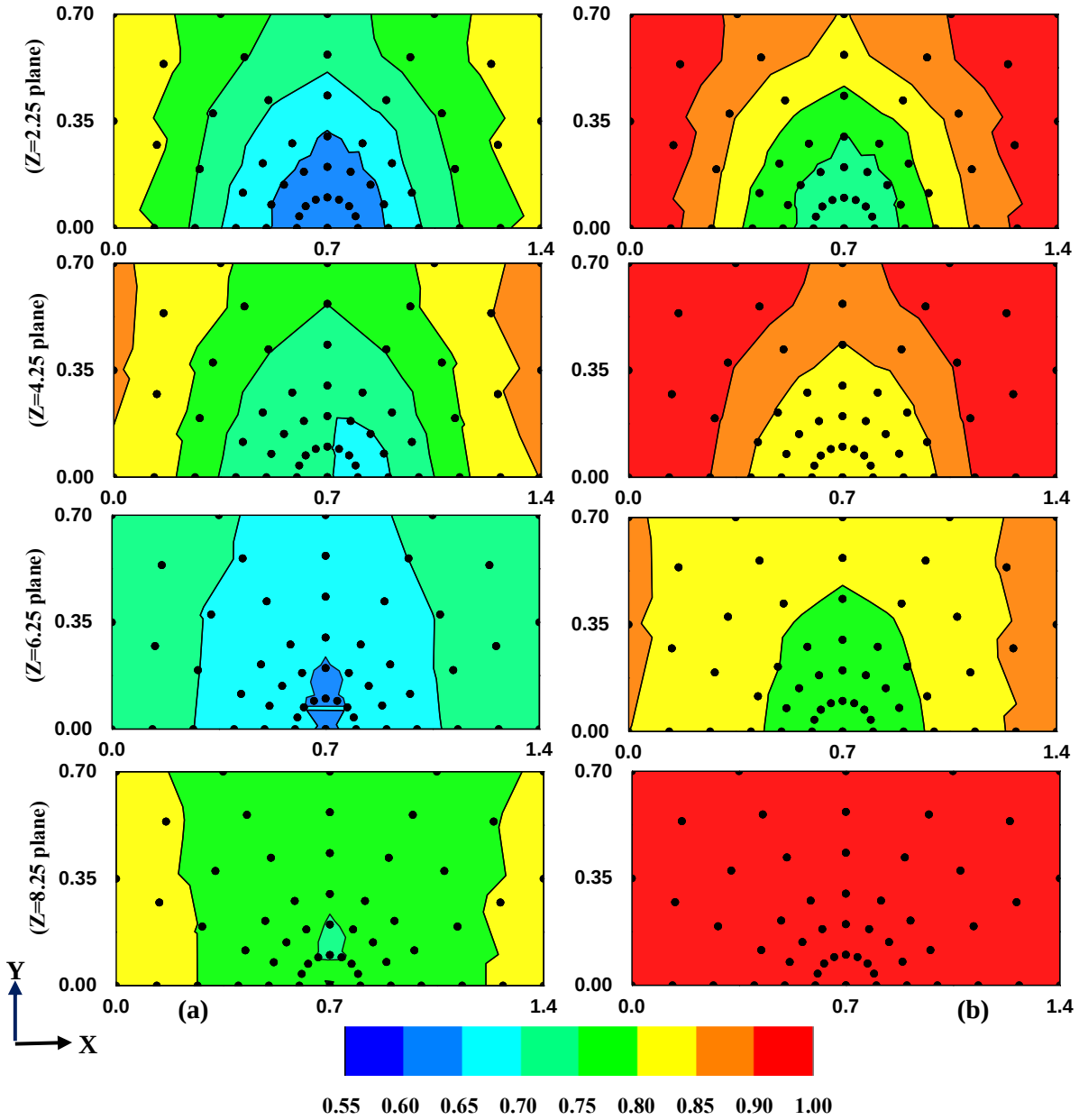

Figure 17. Contours of r_u at different depths (planes Z = 2.25, 4.25, 6.25, and 8.25 m) for the ground treated with granular column: (a) the best performance with smallest ratio of r_u, and (b) the worst performance with largest ratio of r_u from the series of stochastic analyses

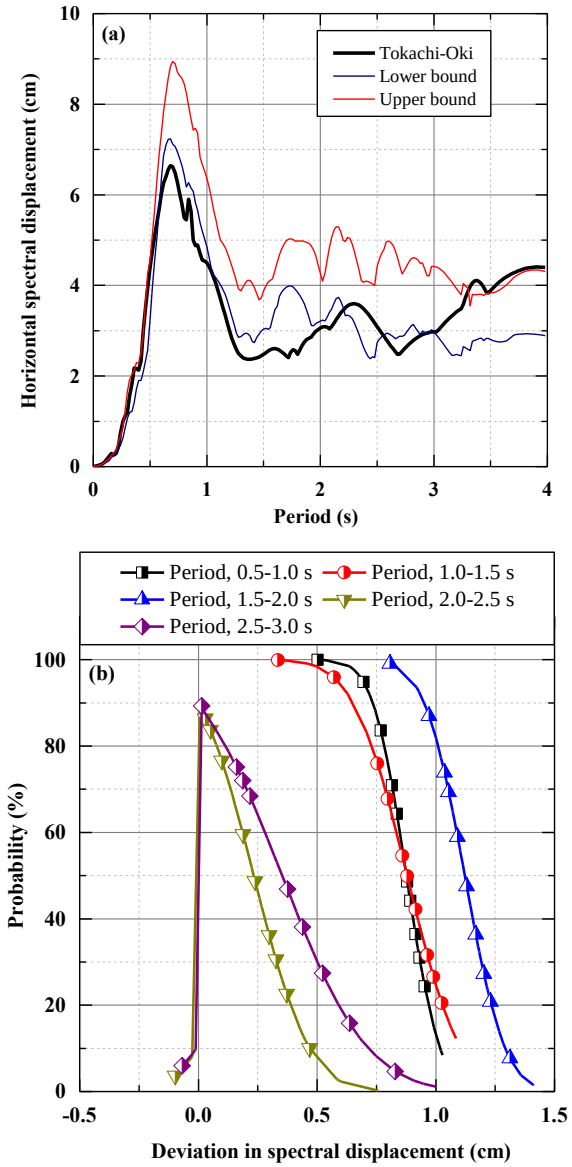

Figure 18. The kinematic response of the ground with granular column: (a) upper and lower bound of displacement response spectra (with 5% damping) at the top surface (Z= 0 m) of the ground and (b) probability of deviation of average spectral displacement (for different period range) from their respective values for Tokachi-Oki ground motion

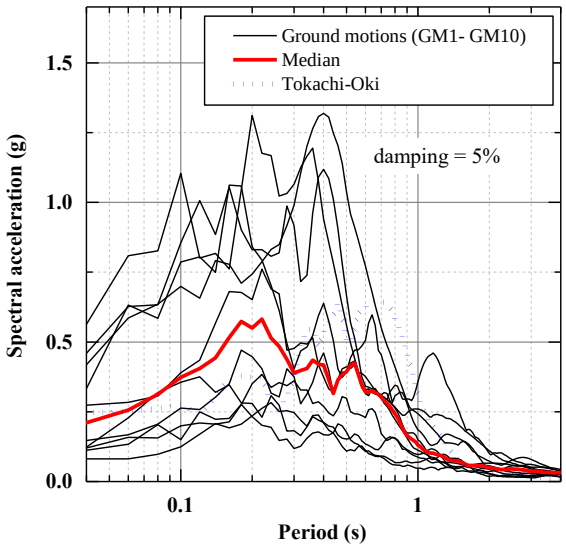

Figure 19. Spectral accelerations for different ground motions (see Table 3)

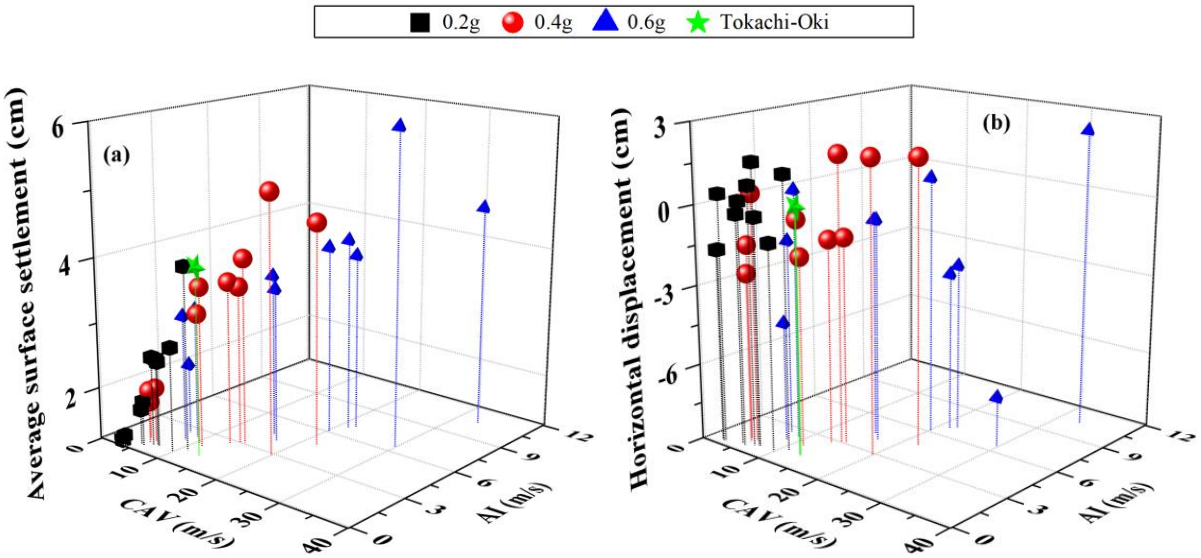

Figure 20. The deterministic response of ten scaled ground motions for the ground with granular column: (a) average surface settlement and (b) surface horizontal displacement

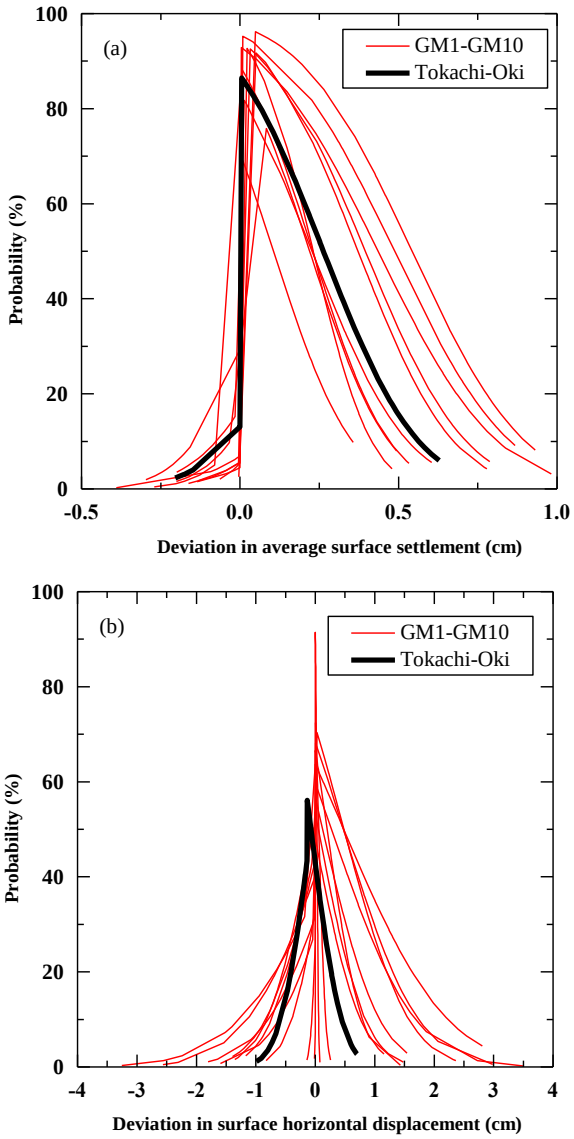

Figure 21. Probability of deviation from the deterministic values for the ground with the granular column for all the ground motions scaled with peak acceleration = 0.6g: (a) for average surface settlement and (b) for surface horizontal displacement